6. SITE 1078[1]

Shipboard Scientific Party[2]

HOLE 1078A

Position: 11°55.2145′S, 13°24.0134′E

Start hole: 2105 hr, 2 September 1997

End hole: 0800 hr, 3 September 1997

Time on hole: 10.92 hr

Seafloor (drill pipe measurement from rig floor, mbrf): 438.5

Total depth (drill pipe measurement from rig floor, mbrf): 515.6

Distance between rig floor and sea level (m): 11.3

Water depth (drill pipe measurement from sea level, m): 427.2

Penetration (mbsf): 77.1

Coring totals:
Type: APC
Number: 8
Cored: 69.5 m
Recovered: 68.9 m (99.07%)

Type: XCB
Number: 1
Cored: 7.6 m
Recovered: 1.5 m (19.86%)

Lithology:
Unit I: olive-gray and dark olive-gray silty clay with varying amounts of nannofossils and foraminifers

HOLE 1078B

Position: 11°55.2318′S, 13°24.0172′E

Start hole: 0800 hr, 3 September 1997

End hole: 1810 hr, 3 September 1997

Time on hole: 10.17 hr

Seafloor (drill pipe measurement from rig floor, mbrf): 437.4

Total depth (drill pipe measurement from rig floor, mbrf): 567.5

Distance between rig floor and sea level (m): 11.3

Water depth (drill pipe measurement from sea level, m): 426.1

Penetration (mbsf): 130.1

Coring totals:
Type: APC
Number: 14
Cored: 130.1 m
Recovered: 125.8 m (96.69%)

Lithology:
Unit I: olive-gray and dark olive-gray silty clay with varying amounts of nannofossils and foraminifers

HOLE 1078C

Position: 11°55.2474′S, 13°24.0161′E

Start hole: 1810 hr, 3 September 1997

End hole: 0535 hr, 4 September 1997

Time on hole: 11.42 hr

Seafloor (drill pipe measurement from rig floor, mbrf): 437.3

Total depth (drill pipe measurement from rig floor, mbrf): 602.5

Distance between rig floor and sea level (m): 11.3

Water depth (drill pipe measurement from sea level, m): 426

Penetration (mbsf): 165.2

Coring totals:
Type: APC
Number: 14
Cored: 128.8m
Recovered: 124.8m (96.9%)

Type: XCB
Number: 4
Cored: 36.4m
Recovered: 24.8m (68.1%)

Lithology:
Unit I: olive-gray and dark olive-gray silty clay with varying amounts of nannofossils and foraminifers

HOLE 1078D

Position: 11°55.2661′S, 13°24.0165′E

Start hole: 0535 hr, 4 September 1997

End hole: 1430 hr, 4 September 1997

Time on hole: 8.92 hr

Seafloor (drill pipe measurement from rig floor, mbrf): 438.7

Total depth (drill pipe measurement from rig floor, mbrf): 565.5

Distance between rig floor and sea level (m): 11.3

Water depth (drill pipe measurement from sea level, m): 427.4

Penetration (mbsf): 126.8

Coring totals:
Type: APC
Number: 14
Cored: 126.8 m
Recovered: 116.71 m (92.04%)

[1]Wefer, G., Berger, W.H., Richter, C., et al., 1998. *Proc. ODP, Init. Repts.,* 175: College Station, TX (Ocean Drilling Program).

[2]Shipboard Scientific Party is given in the list preceding the Table of Contents.

Lithology:

Unit I: olive-gray and dark olive-gray silty clay with varying amounts of nannofossils and foraminifers

Principal results: Site 1078 is located outside the Bight of Angola in 427 m-deep water. Situated between the high-productivity regions off the Congo River to the north and off Namibia to the south, the site is part of a transect that will provide information on "pelagic background" sedimentation for the latest Neogene. Sediments from this region indicate lower primary productivity in overlying waters compared with the adjacent upwelling areas. Thus, the influence of the open ocean is more pronounced and will provide a tie-in of coastal ocean history to the record of the pelagic environment. This will allow us to study the cross-correlations of climate-driven ocean dynamics across these two regimes. One of the intriguing aspects of this record is the low opal content associated with high organic matter accumulation. This paradox indicates a strong influence of the quality of subsurface waters, which is set elsewhere in the system, possibly in the Subtropical Convergence Zone. Other topics of importance are the control of variation by precession, reflecting the changing dominance of trade-wind and monsoonal effects.

Four holes were cored with the advanced hydraulic piston corer/extended core barrel (APC/XCB) at Site 1078 to a maximum depth of 165.2 meters below seafloor (mbsf), which recovered an apparently continuous hemipelagic sedimentary section spanning the last 360 k.y. of the Pleistocene. Hole 1078A was cored with the APC to 69.5 mbsf and deepened with the XCB to 77.1 mbsf. Fourteen APC cores were taken at Hole 1078B to 130.1 mbsf. Hole 1078C was cored with the APC to 128.8 mbsf and deepened with the XCB to 165.2 mbsf. Hole 1078D was cored with the APC to 126.8 mbsf.

Sediments from this site form one lithostratigraphic unit composed predominantly of a moderately bioturbated, olive-gray silty clay with varying amounts of nannofossils and foraminifers. Sediments in the uppermost 3 m contain rare intact gastropod and mollusc shells, pteropods, and abundant shell fragments. Below 80 mbsf, several sections contain whitish gray nodules, 1–2 mm in diameter. Diagenetic dolomite concretions, between 3 and 7 cm thick, and laminated intervals were found at various depths. Calcium carbonate varies between 1 and 25 wt%. The clastic fraction is dominated by smectite, kaolinite and/or illite, quartz, feldspar, and muscovite. The biogenic component is represented by frequent foraminifer fragments and nannofossils. Diatoms are abundant only in laminated sequences. Laminated packages also show abundant diatom resting spores. Trace amounts of plant remains and amorphous organic matter were observed occasionally.

Detailed comparisons between the magnetic susceptibility record generated on the multisensor track (MST) and high-resolution color reflectance measured with the Minolta spectrophotometer demonstrated complete recovery of the sedimentary sequence down to 136 meters composite depth (mcd).

Calcareous microfossils are abundant and well preserved in the entire section, except for the laminated intervals that are barren of nannofossils. Both calcareous nannofossils and planktonic foraminifers show evidence of reworking within the middle part of Hole 1078B. With the exception of the laminated intervals, diatoms, silicoflagellates, and radiolarians are absent at this site. The nannofossil-based biostratigraphy suggests that Site 1078 terminated within the upper half of Zone NN20, between 0.26 and 0.36 Ma.

Assuming a linear sedimentation rate between the two available datum events, sediments accumulated at a rate close to 600 m/m.y. for the interval from 0.09 to 0.26 Ma (Zone NN21a).

Magnetic inclinations and declinations after alternating-field (AF) demagnetization at 20 mT from all four holes indicate that only the Brunhes (C1n) normal polarity Chron is recorded. Short reversal events in the Brunhes Chron were not found, despite the high sedimentation rates.

Sediments average 2.5 wt% total organic carbon (TOC), which is rather high for ocean margin areas and reflects a history of elevated primary production in this area. Interstitial water chemistry studies document a sequence of diagenetic processes caused largely by the degradation of organic matter and carbonate dissolution–reprecipitation reactions. Among these are moderately high levels of methane and carbon dioxide generated by in situ microbial activity. These postdepositional processes are strongly similar to those found at Sites 1075, 1076, and 1077 on the Congo Margin. Profiles of salinity, dissolved chloride, and methane do not indicate the presence of gas hydrate in Site 1078 sediments.

Physical sediment properties were determined both by high-resolution MST core logging and index properties measurements. Magnetic susceptibility and gamma-ray attenuation porosity evaluator (GRAPE) signals reveal pronounced cyclicities, which were used for high-quality stratigraphic correlation in conjunction with digital color data.

The site provides a good high-resolution record for the reconstruction of the oceanography of the Eastern Angola Basin. Of special interest are the changing position of the Angola-Benguela Front and the supply of nutrients from the subsurface waters rising within the Angola Dome. The possibility that silicate content varies through time within that water must be considered; the absence of diatoms, despite high background productivity, is intriguing in this context. Much diatom dissolution takes place during early diagenesis within a zone of high alkalinity generated by sulfate reduction. Occasional development of short laminated sequences (in one case cemented by dolomite) indicates sporadic oxygen deficiency in bottom waters. Possibly, such events are tied to change in the quality of upwelled waters, as suggested by the high abundance of diatoms within laminated sediments. Dolomite layers are present at some depths; several were found near 100 mbsf. Such layers may be important in determining the seismic reflectancy of sediments.

BACKGROUND AND OBJECTIVES

Sites 1078 and 1079, within the Bight of Angola, were chosen as part of a transect planned to provide information on "background" sedimentation that is unaffected by coastal upwelling for the latest Neogene, between the high-productivity regions to both the north and south. The region is characterized by salt tectonics and is being explored for hydrocarbon potential, especially to the north. Permission to drill other sites along the planned transect was thus denied because of safety concerns. The two remaining shallow sites, being very close to shore, are not typical for "background sedimentation."

Earlier studies (e.g., Wefer et al., 1988) established that compared with the adjacent upwelling areas, sediments from this region indicate low primary productivity in overlying waters. Unlike off northern Angola, where the estuarine dynamics of the Congo are dominant, and off Namibia, where upwelling is strong year-round, upwelling of subsurface waters is seasonal here and relatively weak. Thus, the influence of the open ocean is more pronounced at Sites 1078 and 1079 and provides a tie-in of coastal-ocean history to the record of the pelagic environment.

The region is part of a large complex of fronts, gyres, and thermal domes, which reflect the interactions of the trade-wind-driven South Equatorial Current and the eastern boundary currents along southwest Africa: the Angola and Benguela Currents. In analogy to the eastern tropical Pacific, the interactions between these currents result in open-ocean and coastal upwellings over large areas within a highly productive region (van Bennekom and Berger, 1984; Jansen and van Iperen, 1991). Within that complex, the sites selected for drilling are situated in an island of relatively low productivity (Fig. 1).

The general level of primary productivity in the Eastern Angola Basin is between 125 and 180 g C/m^2/yr, with the higher values occurring close to shore (Berger and Wefer, 1991). Silicate values are low in the subsurface Benguela Current, which flows northward and feeds the oceanic upwelling area off Angola. The low silicate supply from subsurface waters results in relatively low opal production rates, despite the high primary production, with high organic carbon

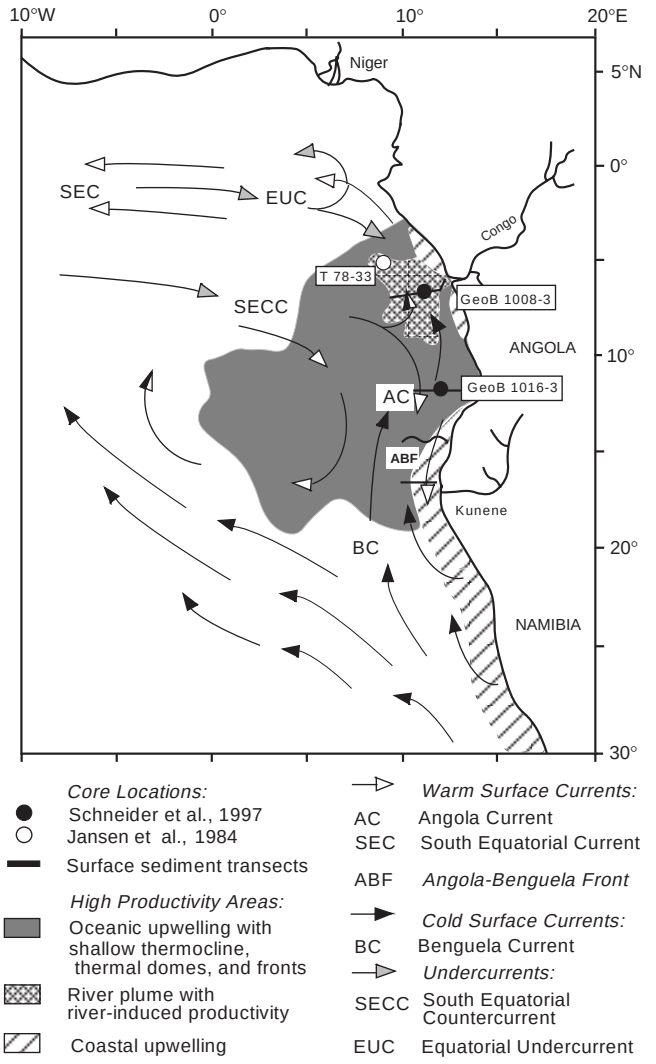

Figure 1. Main surface and subsurface currents and areas with high primary productivity in the southeast South Atlantic (from Schneider et al., 1997).

export. This export relies mainly on the contributions from coccolithophores and dinoflagellates, which characterize the phytoplankton community in the oceanic upwelling area off Angola (Hentschel, 1933; Shannon and Pillar, 1986).

A core taken near the drill sites (Geosciences Bremen [GeoB] 1016-3; water depth 3441 m; Wefer et al., 1988) shows paleoproductivity changes related to precessional cycles. These cycles influence upwelling via trade-wind-forced shallowing of the thermocline and nutricline and by changing advection of cold Benguela Current waters from the south (Schneider et al., 1997). Lack of silica, as at present, has prevented significant accumulation of opal in these sediments for at least the last 300,000 yr. As a result, fluctuations (such as might be expected from glacial/interglacial cycles) are greatly subdued, despite considerable variation in the abundance of total organic carbon (Fig. 2). Schneider et al. (1997) conclude from this evidence that during this time period, the Namibian coastal upwelling cell has never made its influence known this far north.

We expect a close tie-in of climatic records of coastal and open ocean in this area, allowing us to study the cross-correlations of climate-driven ocean dynamics across these two regimes. Previous work on Pleistocene sediments in the region (Schneider et al., 1997) has shown that an excellent record with good time resolution can be expected for the purpose of relating pelagic stratigraphy to the record of the coastal ocean. One of the intriguing aspects of this record is the low opal content associated with high organic matter accumulation. This paradox indicates a strong influence of the quality of subsurface waters, which is set elsewhere in the system, possibly in the Subtropical Convergence Zone. Other topics of importance are the control of variation by precession, reflecting the changing dominance of trade-wind and monsoonal effects.

OPERATIONS

Hole 1078A (Proposed Site MAB-1)

The vessel proceeded directly to the Global Positioning System coordinates of Site 1078, where a beacon was deployed at 2105 hr on 2 September. The bit was positioned at 436.5 m, where Hole 1078A was spudded at 0040 hr on 3 September. The seafloor depth was established at 627.2 meters below sea level (mbsl) by drill-pipe measurement (DPM). APC Cores 175-1078A-1H through 8H were taken from 0 to 77.1 mbsf (Table 1; also see expanded core summary table on CD-ROM, back pocket, this volume), which was considered APC refusal (recovery 100.4%). During the firing of Core 8H, a lock pin failed and left part of the sinker bar assembly and the core barrel at the bottom of the drill string. It required three wireline fishing attempts to recover the sinker bar hardware and another wireline trip to recover the full core barrel. The Adara heat-flow shoe was deployed with Cores 3H (26.5 mbsf) and 6H (55.0 mbsf). An XCB core (175-1078A-9X) advanced the hole to 77.1 mbsf with 20% recovery. This was considered the total depth of the hole. The drill string was pulled back with the bit clearing the seafloor at 0800 hr on 3 September, thereby ending Hole 1078A.

Hole 1078B

The vessel was offset 30 m to the south, and Hole 1078B was spudded at 0837 hr on 3 September. The seafloor depth was established at 426.1 mbsl by DPM. APC Cores 175-1078B-1H through 14H were taken from 0 to 130.1 mbsf (Table 1), with 130.1 m cored and 125.7 m recovered (96.6% recovery). Cores were oriented starting with Core 3H. The Adara heat-flow shoe was deployed with Cores 11H (101.6 mbsf) and 14H (130.1 mbsf). The drill string was pulled out of the hole and cleared the seafloor at 1810 hr on 3 September, ending Hole 1078B.

Hole 1078C

The vessel was offset 30 m to the south, and Hole 1078C was spudded at 1905 hr on 3 September. The seafloor depth was established at 426.0 mbsl by DPM. APC Cores 175-1078B-1H through 14H were taken from 0 to 128.8 mbsf (Table 1) and were deepened with the XCB to 165.2 m, with 165.2 m cored and 149.6 m recovered (90.5% recovery). Cores were oriented starting with Core 3H. The drill string was pulled out of the hole and cleared the seafloor at 05.35 hr on 4 September, ending Hole 1078C.

Hole 1078D

Once again, the vessel was offset 30 m to the south, and Hole 1078D was spudded at 0605 hr on 4 September. The seafloor depth was established at 427.4 mbsl by DPM. APC Cores 175-1078B-1H through 14H were taken from 0 to 126.8 mbsf (Table 1), with 126.8 m cored and 116.7 m recovered (92.1% recovery). Cores were not oriented. The drill string was pulled out of the hole and cleared the seafloor at 1300 hr on 4 September, ending operations at Site 1078.

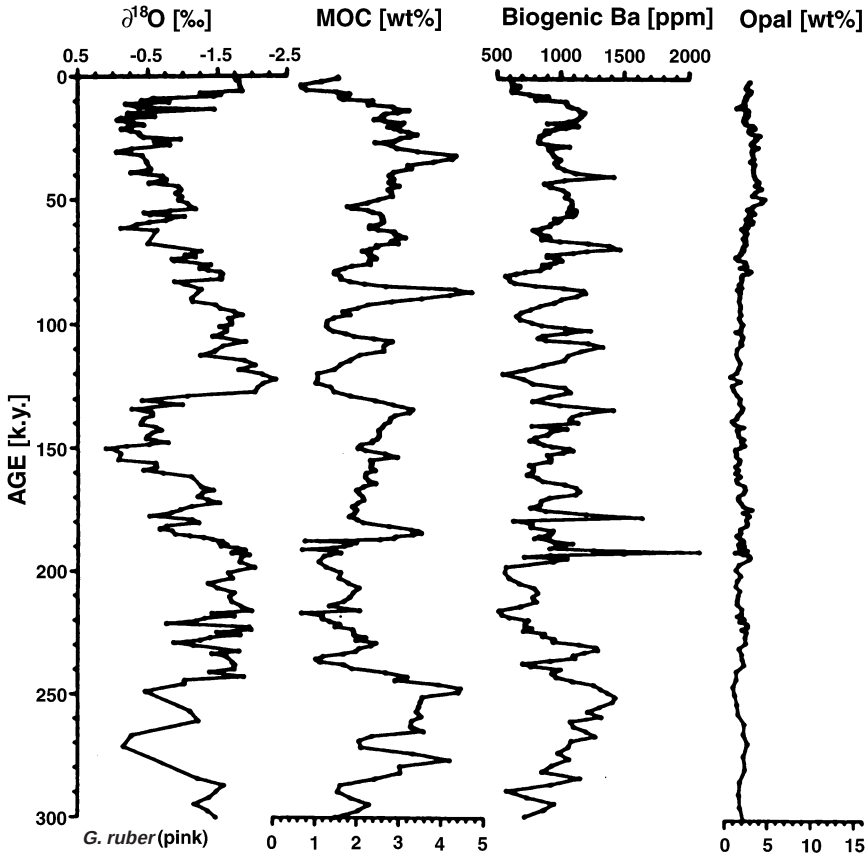

Figure 2. Variations of marine organic carbon (MOC) and opal weight percentage, as well as of biogenic barium in parts per million (ppm) in Angola margin sediments over the last 300,000 yr. For stratigraphic purposes, the oxygen isotopes of *Globigerinoides ruber* (pink) are shown. Locations of Cores GeoB 1008-3, GeoB 1016-3, and T78-33 used in the study are also shown (modified from Schneider et al., 1997).

SITE GEOPHYSICS

Introduction and Strategy

The second working area of Ocean Drilling Program (ODP) Leg 175 was located on the marginal plateau off the coast of Angola at 12°S. The area lies between the Congo River and the Angola-Namibia upwelling cell. Major scientific targets are based on the assumption that the location represents a (hemi-) pelagic depositional regime with respect to biogenic sediment input, which is still under the influence of the Benguela Current, but is typical for open-ocean conditions. The sites are suitable to monitor variations in the Angola-Benguela Front. Sedimentation rates are expected to be generally lower than in the Congo Fan area because of reduced coastal upwelling and the lack of large river systems in the area. To explain the strategy of the site survey (Bleil et al., 1995), a short summary of the evidence regarding the expected sedimentary structures at this part of the continental margin is given.

The regional morphology is controlled by a rift basin, which developed during the early opening of the South Atlantic. In Aptian–Albian times, a shallow-water basin was repeatedly flooded, and evaporitic layers of altogether several hundred meters in thickness accumulated (Baumgartner and van Andel, 1971; Leyden et al., 1972; Emery et al., 1975; Emery and Uchupi, 1984). The subsequent phase of seafloor spreading disrupted this basin. A major portion between the equator and ~13°S remained at the African continental margin, forming a plateau in water depths shallower than 2500 to 3000 m. Its seaward boundary, the Angola Escarpment, can be traced as a prominent morphological and structural feature (Fig. 3).

Soon after deposition of the salt layers, buoyant forces initiated vertical movements, which are also observed in the coastal basins (Brice et al., 1982; Emery et al., 1975). They continued during the Late Cretaceous and Cenozoic, when several kilometers of sediments were accumulated on the continental margin and the plateau. This salt tectonism has shaped the morphology of the area and dominates the regional sedimentation pattern. Numerous diapiric structures in the relict rift basin were imaged and analyzed in some detail by the seismic surveys of Baumgartner and van Andel (1971), Leyden et al. (1972), and Brice et al. (1982). Intensive salt tectonism is associated with the diapirism. Because of the short average distance between diapirs, the identification of suitable potential drill sites with undisturbed sedimentary sequences was rather complicated. Also, because of the hydrocarbon potential associated with black shales and salt, the area became of great interest to the oil industry. In recent years, intensive seismic surveying has started; however, given that concessions are still being negotiated, this information is not yet accessible to the public.

The preliminary site proposals in this region were based on seismic Line 44 of Emery et al. (1975), but the data quality was not sufficient to identify fine-scale sedimentary structures and to prove the absence of disturbances. Based on recent bathymetric data, the relatively complex topographic structures around this profile were avoided, and the survey area was moved south to ~12°S. All drill sites proposed here (Fig. 3) are positioned on Line GeoB/AWI 93-015 (Fig. 4), for which six crossings are available. Additional high-resolution seismic profiles were recorded across Deep Sea Drilling Project (DSDP) Sites 364 and 365 (Bolli, Ryan, et al., 1978) to establish a seismostratigraphic correlation with the former drilling results.

Bathymetric data acquired with the Hydrosweep swath sounder system show that water depths in the selected area are <2000 m. West of ~12°40′E on the outer plateau, and less pronounced on the inner plateau to ~12°50′E, the morphology is irregular with slightly elongated north-northwest/south-southeast trending features of 50- to 100-m amplitude. Salt diapirism, which reaches close to the surface and thereby also affects the topography, has created this sequence of peaks and troughs. As the basins between the diapiric structures are

Table 1. Coring summary for Site 1078.

Core	Date (Sept. 1997)	Time (UTC)	Interval (mbsf)	Length cored (m)	Length recovered (m)	Recovery (%)
175-1078A-						
1H	3	0045	0.0-7.5	7.5	7.45	99.3
2H	3	0115	7.5-17.0	9.5	8.85	93.2
3H	3	0200	17.0-26.5	9.5	8.88	93.5
4H	3	0225	26.5-36.0	9.5	8.42	88.6
5H	3	0250	36.0-45.5	9.5	9.61	101.2
6H	3	0335	45.5-55.0	9.5	10.90	114.7
7H	3	0400	55.0-64.5	9.5	9.72	102.3
8H	3	0620	64.5-69.5	5.0	4.94	98.8
9X	3	0720	69.5-77.1	7.6	1.51	19.9
Coring totals:				77.1	70.28	91.2
175-1078B-						
1H	3	0845	0.0-6.6	6.6	6.66	100.9
2H	3	0910	6.6-16.1	9.5	9.80	103.2
3H	3	0935	16.1-25.6	9.5	9.95	104.7
4H	3	1005	25.6-35.1	9.5	10.06	105.9
5H	3	1030	35.1-44.6	9.5	10.20	107.4
6H	3	1100	44.6-54.1	9.5	9.01	94.8
7H	3	1125	54.1-63.6	9.5	10.81	113.8
8H	3	1205	63.6-73.1	9.5	11.22	118.1
9H	3	1245	73.1-82.6	9.5	10.17	107.1
10H	3	1320	82.6-92.1	9.5	6.94	73.1
11H	3	1405	92.1-101.6	9.5	10.00	105.3
12H	3	1445	101.6-111.1	9.5	7.43	78.2
13H	3	1520	111.1-120.6	9.5	6.25	65.8
14H	3	1620	120.6-130.1	9.5	7.30	76.8
Coring totals:				130.1	125.80	96.7
175-1078C-						
1H	3	1905	0.0-6.7	6.7	6.71	100.1
2H	3	1935	6.7-16.2	9.5	9.83	103.5
3H	3	2015	16.2-25.7	9.5	10.14	106.7
4H	3	2040	25.7-35.2	9.5	9.69	102.0
5H	3	2110	35.2-44.7	9.5	10.04	105.7
6H	3	2140	44.7-54.2	9.5	9.52	100.2
7H	3	2210	54.2-63.7	9.5	10.14	106.7
8H	3	2245	63.7-73.2	9.5	8.76	92.2
9H	3	2315	73.2-82.7	9.5	9.09	95.7
10H	3	2350	82.7-92.2	9.5	3.63	38.2
11H	4	0020	92.2-101.7	9.5	10.20	107.4
12H	4	0050	101.7-111.2	9.5	8.36	88.0
13H	4	0120	111.2-120.7	9.5	10.53	110.8
14H	4	0200	120.7-128.8	8.1	8.14	100.5
15X	4	0315	128.8-136.2	7.4	5.61	75.8
16X	4	0345	136.2-145.9	9.7	4.18	43.1
17X	4	0415	145.9-155.5	9.6	9.52	99.2
18X	4	0435	155.5-165.2	9.7	5.49	56.6
Coring totals:				165.2	149.58	90.6
175-1078D-						
1H	4	0610	0.0-7.3	7.3	7.35	100.7
2H	4	0630	7.3-16.8	9.5	9.96	104.8
3H	4	0655	16.8-22.3	5.5	5.86	106.5
4H	4	0710	22.3-31.8	9.5	10.08	106.1
5H	4	0725	31.8-41.3	9.5	9.90	104.2
6H	4	0745	41.3-50.8	9.5	10.10	106.3
7H	4	0805	50.8-60.3	9.5	7.51	79.1
8H	4	0835	60.3-69.8	9.5	10.07	106.0
9H	4	0855	69.8-79.3	9.5	6.13	64.5
10H	4	0920	79.3-88.8	9.5	7.73	81.4
11H	4	1010	88.8-98.3	9.5	8.94	94.1
12H	4	1030	98.3-107.8	9.5	9.61	101.2
13H	4	1115	107.8-117.3	9.5	3.25	34.2
14H	4	1200	117.3-126.8	9.5	10.22	107.6
Coring totals:				126.8	116.71	92.0

Notes: UTC = Universal Time Coordinated. An expanded version of this coring summary table that includes lengths and depths of sections and comments on sampling is included on CD-ROM (back pocket, this volume).

only ~10 km wide, appropriate locations for first priority paleoceanographic drill sites could not be identified. East of 12°50′E, the upper continental slope is smooth.

Seismostratigraphy

Altogether, 16 seismic lines were recorded in the Mid-Angola Basin area, with six crossings at potential drill sites in water depths between 550 and 1460 m along Line GeoB/AWI 93-015 (Fig. 3). Line GeoB/AWI 93-014 was shot to link the drilling results of DSDP Leg 40 (Sites 364 and 365) with the new findings of this leg. It turns out, however, that seismic characteristics at the DSDP sites and in the working area were different. Accordingly, it must be concluded that the depositional pattern is different, probably because of significantly enhanced terrigenous input in the Leg 175 working area. Recordings at Line GeoB/AWI 93-017 revealed a mostly disturbed sedimentary section, indicating a mass flow probably originating from the shelf area in the south. On Line GeoB/AWI 93-029, it could be confirmed that these mass-flow deposits extend into the Angola Basin, and no hemipelagic sequences suitable for drilling were identified.

Vertical salt movements (the predominant tectonic process in the area) have directly affected the regional morphology and sediment deposition. In the western part of the plateau, diapiric structures nearly reach the surface. The sediment structures on top and on the flanks are deformed, indicating postdepositional salt tectonics. Figure 4 shows the eastern portion of Line GeoB/AWI 93-015, which lies east of the diapiric zone (Baumgartner and van Andel, 1971) where the influence of salt tectonism in the surface sediments is of minor importance. Only smooth changes in near-surface reflection patterns are observed on this line, indicating the absence of significant mass-flow deposition.

For safety and pollution considerations, only two of six proposed sites were approved, and penetration was limited to 200 and 120 m, respectively. This restriction was based on the analyses of reflection amplitudes, which appear to be very high and sometimes reveal some scattering in the surface sediments. Furthermore, numerous pockmarks downslope at proposed sites MAB 5A and 5B strongly indicated fluid and/or gas migration. Besides a salt diapir around common depth point (CDP) 7500 and further evidence for diapirs on crossing lines north and south of Line GeoB/AWI 93-015, indications for shallow gas were found between CDPs 7800 and 8050 and for deeper gas accumulation between CDPs 6300 and 6600 and CDPs 6800 and 7200. Seismic reflectors of pronounced lateral variability in amplitude exist in the vicinity of all proposed sites, but were less disturbed for the uppermost two sites.

A subdivision into seismostratigraphic units here is less straightforward than in the Lower Congo Basin. Reflectors in the uppermost 300 ms two-way traveltime (TWT) at Site 1079 and 500 ms TWT at Site 1078 appear to be very coherent and can be easily correlated between the sites. Beneath this zone, which could not be reached by drilling, a nearly transparent interval from 200 ms TWT (CDP 6300) to 500 ms TWT (Site 1078) appears.

The uppermost band of reflectors can be subdivided into two seismostratigraphic units, which were reached by drilling and will be described for the vicinity of the two drill sites.

Seismostratigraphic Unit 1

The uppermost Unit 1 of 120 to 160 ms TWT reveals a coherent reflection pattern with a high-amplitude reflector at the surface and the base, which, however, decreases in amplitude upslope. Within this unit, amplitudes are generally weak with minor lateral changes between the sites, except for a stronger reflector at 100 ms TWT at Site 1078, which is less pronounced downslope at Site 1079. The distance between individual reflectors varies, indicating minor slumping units.

Seismostratigraphic Unit 2

Beneath the base reflector of Unit 1, amplitudes are generally weaker. Some reflectors are interrupted by transparent or disturbed zones. The thickness of the unit varies from 60 to 100 ms TWT, and its base is again defined by a stronger, continuous reflector. Beneath it, a local amplitude anomaly, which is associated with a thickening, is found between the two sites. Beneath seismostratigraphic Unit 2,

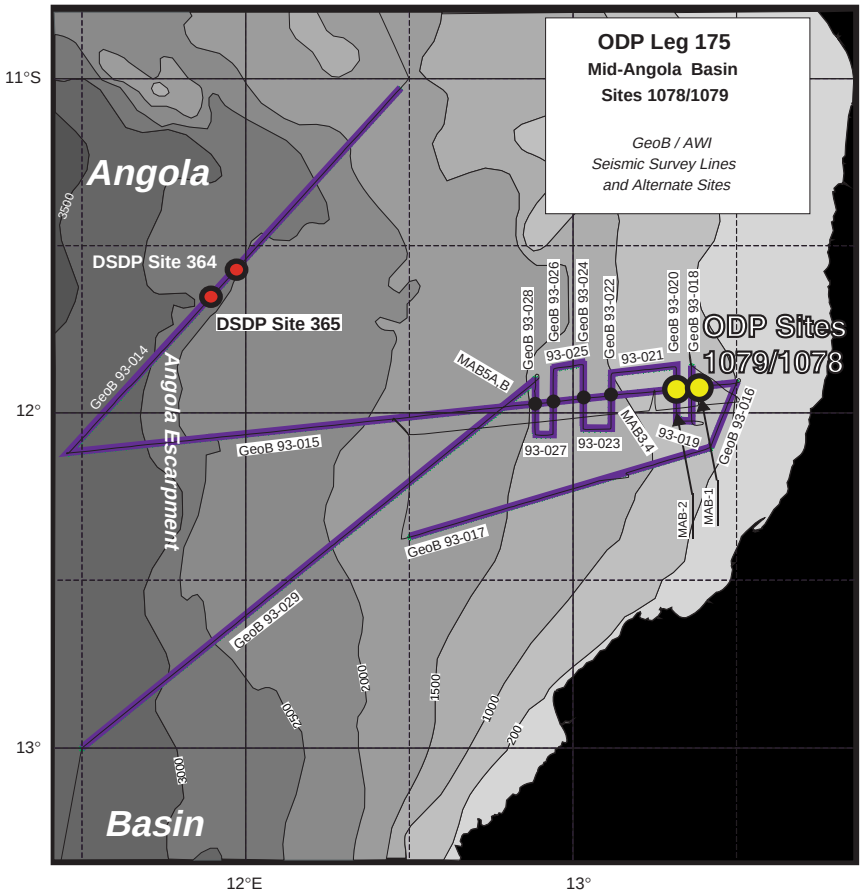

Figure 3. Map of seismic presite survey lines, proposed site locations, and ODP Leg 175 drill Sites 1078 and 1079 in the Mid-Angola Basin. Bathymetry was derived from the Gebco Digital Dataset on CD-ROM.

scatter increases significantly and is interpreted as a potential indicator for shallow gas leading to the restriction in drilling depth. Alternatively, the scatter could be caused by irregular surfaces of slump units.

The basic assumption that the sedimentary sequences at the margin are not dominated by mass-flow deposits and that deposition is generally hemipelagic, as was found for the Lower Congo Basin, could be confirmed by the seismic survey. Although a sufficient number of sites were proposed to study a transect in water depth and distance from the shelf, safety considerations limited the drilling program to the shallowest sites at 432 and 738 m water depth, respectively.

Site 1078

Site 1078 was located in 426 m water depth at the eastern end of the survey area on Line GeoB/AWI 93-015 (CDP 8550). Figure 5 shows a 10-km-long seismic section of Line GeoB/AWI 93-015 across Site 1078. Weak reflectors were enhanced by normalization of amplitudes to a constant value. Therefore, the general characteristics described for the seismic units do not appear as pronounced as they would in a color-coded section. But the figure confirms the separation into two units within the proposed drilling depth range. Regarding distance from the shelf, the site is located where most of the sedimentary units are thickest, providing the highest sedimentation rate in the area within the upper 200 m. However, it cannot be excluded that the thickening is at least partially attributed to thin mass-flow deposits.

Significantly disturbed and scattering intervals are found beneath 200 m, and a sharp transition in reflectivity at a depth of 530 ms TWT. The site was moved from the originally proposed location to avoid the amplitude anomaly between CDPs 8370 and 8500 at a depth of about 300 ms TWT.

Figure 6 shows a close-up of the seismic section, plotted against sub-bottom depth for a sound velocity of 1500 m/s, for a 1-km-long interval in the vicinity of the drill site. Seismic reflectors are compared with the smoothed GRAPE density core log for Hole 1078C. Seismograms are plotted as wiggle traces with gray-scaled amplitudes as background. Laminated intervals are indicated by a thick arrow, and "D" indicates documented dolomite layers or dolomitic clays. Small arrows are plotted at depth where one or a few anomalously high GRAPE readings were found in any of the four holes (1800 to 2400 kg/m^3). These density anomalies have different origins: stones at 8–9 mbsf, silty bands at 38.7 or 43.8 mbsf, an (erosional) contact at 55.1 mbsf, or dolomite at 82.9 mbsf. Depending on their thickness and distribution, they are potential candidates for seismic reflectors, but some of them might only be visible in ultra-high-resolution seismic data from echosounders. Selected reflectors can be directly correlated with sharp changes in the density log, but the seismic wavelength is not short enough to uniquely distinguish individual reflectors from interference patterns. The probably compaction-related density gradient in the upper 10 m results in a significant decrease of the surface reflection amplitude, which, in turn, would affect the evaluation of deeper reflector amplitudes. Such a gradient was not observed in sediments from the Lower Congo Basin.

Because of the lack of logging data, it is not possible to state at this point whether high amplitudes are generally associated with levels of dolomitization. There is no direct correlation between the presence of dolomitized layers in the sediment and reflection amplitudes. This would imply that either the distribution of dolomites is nodular and does not affect the seismic wave significantly, or the thickness is

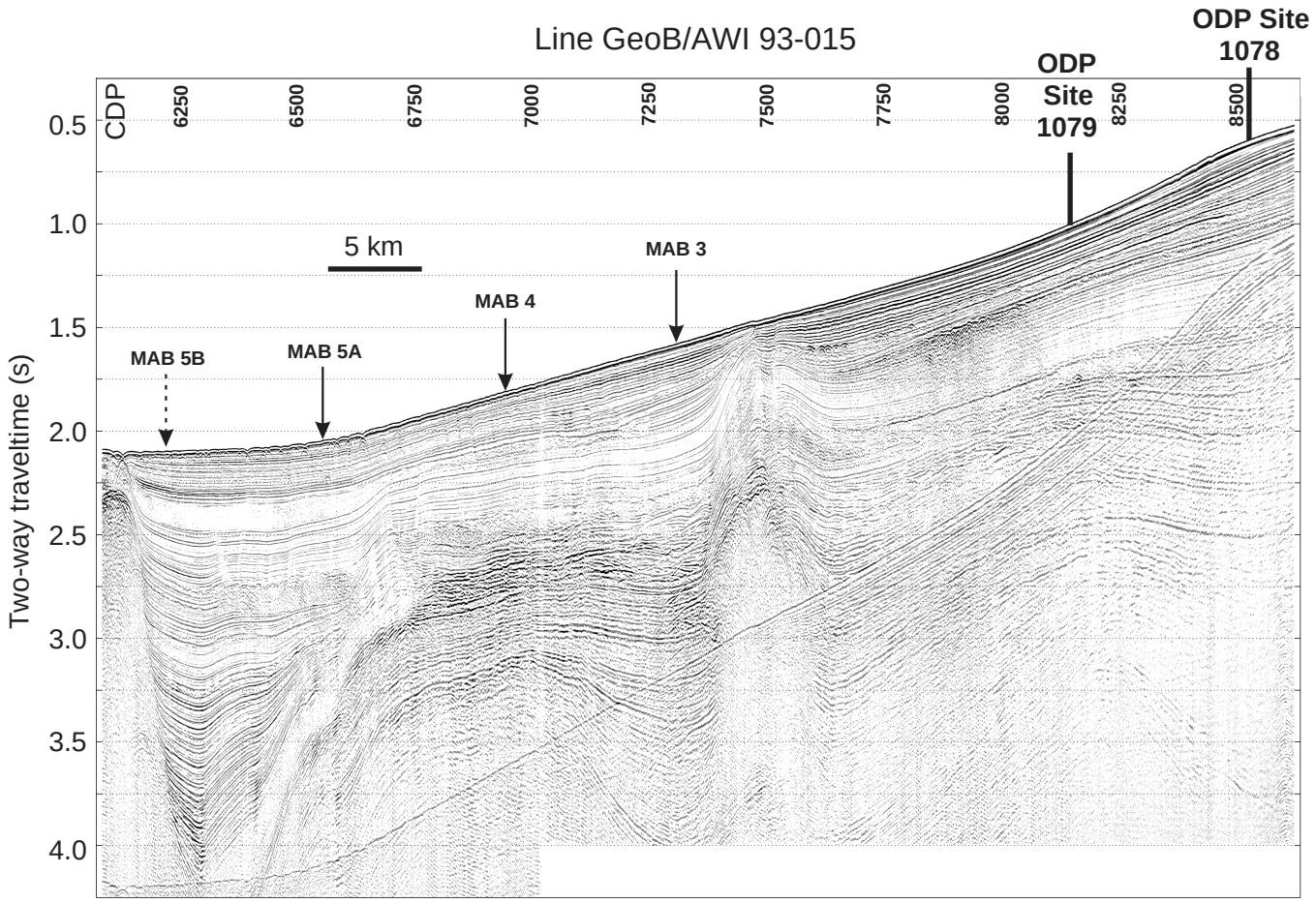

Figure 4. Seismic Line GeoB/AWI 93-015 at Sites 1078 and 1079. Vertical axis is given in two-way traveltime. Common depth point (CDP) interval is 25 m for a shotpoint spacing of 25 m. Seismic data is 24-fold stacked and not migrated. Site 1078 is located at CDP 8550; Site 1079 at CDP 8150. Four additional sites (MAB 3, 4, 5A, 5B) were originally proposed; one (MAB 5B) was withdrawn before the safety review.

too small to generate a high-amplitude echo. A regional analysis of amplitudes in the vicinity of the drill sites is intended to further elucidate the presence and distribution of dolomitization. Where reflectors are coherent and of constant amplitude, dolomitized layers must be assumed to have a major impact on migratory processes of gas and fluid in the sediment, as well as the trapping of shallow gas and hydrocarbons. The low reflectivity beneath 530 ms TWT can be explained only by the absence or dissolution of dolomitized layers, a drastic overall change in lithology, or an overprint of reflection amplitude caused by the presence of gas and/or fluids. So far, no evidence can be derived from the shallow drill holes to explain the observed variations.

Laminated intervals appear as low-amplitude, but consistent, reflectors in the multichannel seismic data and might be used as stratigraphic markers. The digital echosounder can be used in shallow depths to analyze the regional distribution of this sedimentation event. Calculation of synthetic seismograms from calibrated and spliced GRAPE data sets is required to carry out more detailed analyses. The required thorough editing and quality control can be carried out only on shore.

Site 1079

Site 1079 is located downslope of Site 1078 in a water depth of 738 m and at CDP 8150 of Line GeoB/AWI 93-015. Figure 7 shows a 10-km-long section of seismic Line GeoB/AWI 93-015 close to the drill site. Drilling was approved down to 120 mbsf, as discussed above. The transition between the two seismostratigraphic units can be reached at ~120 ms TWT. The upper sedimentary sequence appears ~25% thinner than that at Site 1078. At Site 1079, disturbances in greater depth are generally more pronounced and reveal hyperbolic echoes. The strong reflector denoting the transition between higher and lower reflective zones is overprinted by seismic scatter downslope, which could suggest shallow gas accumulation.

The 1-km-long close-up section near the drill site is shown in Figure 8. Seismic reflectors are compared with the wet bulk density log, derived from index properties measurements (see “Physical Properties” section, “Site 1079” chapter, this volume). Numerous reflectors could be assigned to sharp changes in physical properties, but additional reflectors might derive from the interference of seismic waves at closely spaced variations in acoustic impedance. In contrast to Site 1078, evidence for a lithified dolomitic layer was not found at Site 1079. An accumulation of silty bands was reported at a depth of ~85 mbsf, which might be assigned to a regionally correlatable reflector. The transition between seismostratigraphic units can be explained by a generally decreased scatter in the data, which leads to subdued reflection amplitudes and reduced interference.

A correlation of core data with seismograms awaits further editing of MST measurements and calculation of synthetic seismograms based on cleaned and spliced data sets.

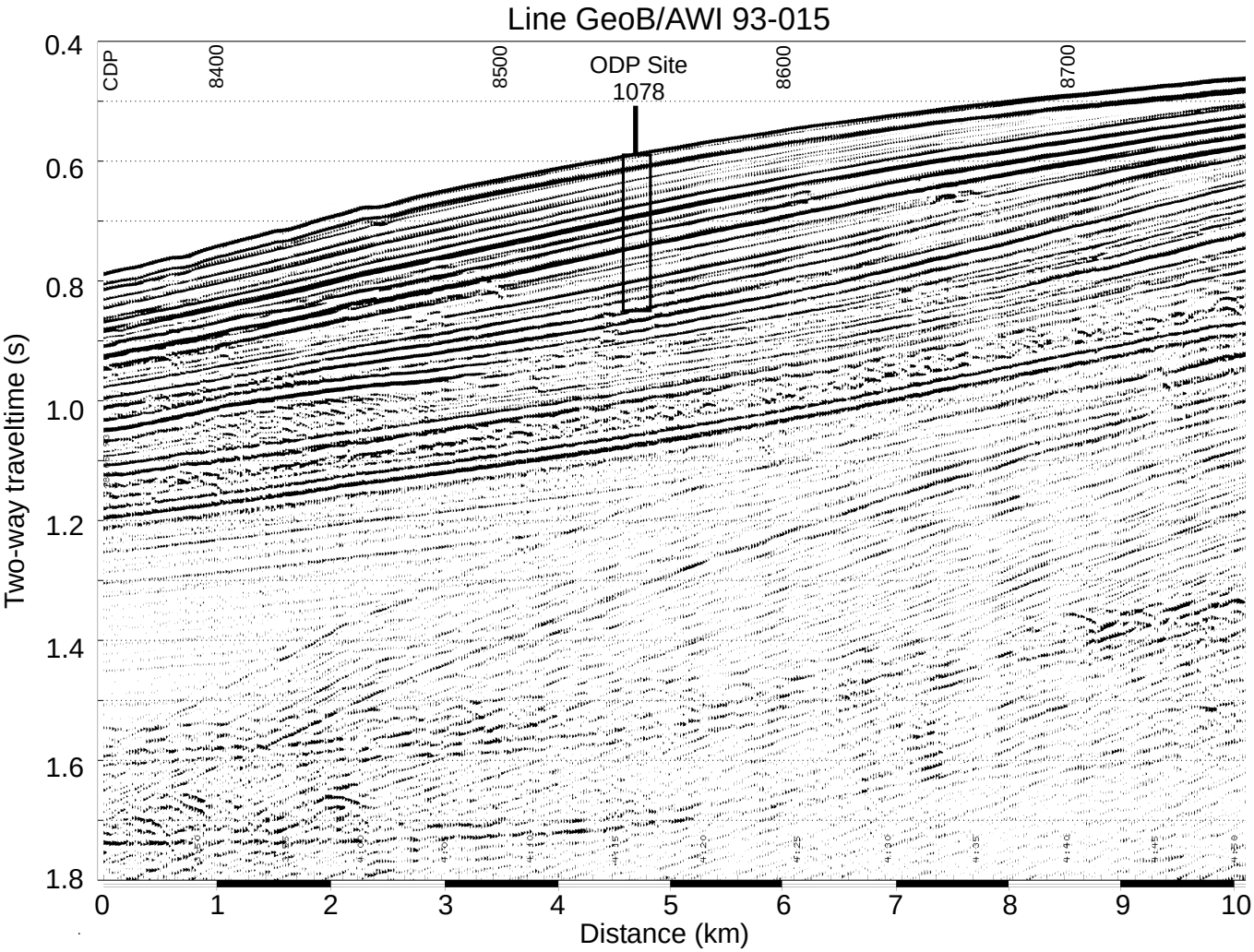

Figure 5. Seismic section of line GeoB/AWI 93-015 at Site 1078. Vertical axis is given in two-way traveltime. CDP interval is 25 m for a shotpoint spacing of 25 m. Site 1078 is located at CDP 8550. The box indicates the approximate penetration of the borehole of 200 m.

LITHOSTRATIGRAPHY

Introduction

Four holes were drilled at Site 1078 with the APC/XCB to a depth of 165.2 mbsf. Several sections showed flow-in structures that were observed as pseudo-bedding parallel to the core liner and multiple stacked cones. Sedimentological data from suspect sections generally support paleomagnetic and biostratigraphic data, and affected sections were marked on the barrel sheets. In general, sections in the last cores before APC refusal (i.e., 175-1078A-7H-6, 5H-7, 6H-6, 7H-5, 8H-6, 9H-7, 11H-6, 12H-5; 175-1078C-11H-6, 13H-6; and 175-1078D-7H-4) are suspected to be affected by flow-in. Additional core disturbances were common in the uppermost 20 cm of many cores.

Description of Lithostratigraphic Unit

Sediments from Site 1078 form one lithostratigraphic unit composed predominantly of a moderately bioturbated, olive-gray (5Y 4/2) and dark olive-gray (5Y 3/2) silty clay with varying amounts of nannofossils and foraminifers (Fig. 9). Light olive-gray (5Y 6/2), 0.5- to 1.0-cm-thick, silt-rich layers with diffuse contacts are sometimes interbedded within some bioturbated intervals. Sediments in the uppermost three sections of all holes contain rare intact gastropod and mollusc shells, pteropods, and abundant shell fragments. Below 80 mbsf, all holes contain several sections with whitish gray nodules, 1–2 mm in diameter (Fig. 10). Diagenetic dolomite horizons between 3 and 7 cm in thickness are present in Sections 175-1078C-13H-1, 175-1078C-15X-3, and 175-1078D-10H-3 (Fig. 11). Calcium carbonate content ranges from 1 to 25 wt% but are typically between 17 and 20 wt% of the sediment (Fig. 9).

A 40-cm-thick laminated sequence rich in diatoms (see “Biostratigraphy and Sedimentation Rates” section, this chapter) is present in Sections 175-1078A-5H-3, 175-1078B-5H-4, and 175-1078C-5H-4 (Fig. 12). A comparable but less well-laminated sequence is also present in Section 175-1078D-5H-6. Stratigraphic data suggest that the laminated sediments at this depth extend laterally over some distance and are a useful marker horizon for correlation between holes. Two additional, 26- and 40-cm-thick, laminated sequences are present in intervals 175-1078C-15X-2, 114–140 cm, and 175-1078C-15X-3, 30–70 cm (Fig. 13). The laminated sequences are composed of diatom-rich, alternating dark olive-gray and dark gray layers 1–3 mm in thickness. Thinner laminae are discontinuous, extending only 5–20 mm. Bioturbated silty clay intervals are common at the top and bottom of the laminated sequences, which suggests that a lack of oxygen was crucial for the preservation of laminated intervals by the exclusion of burrowing organisms.

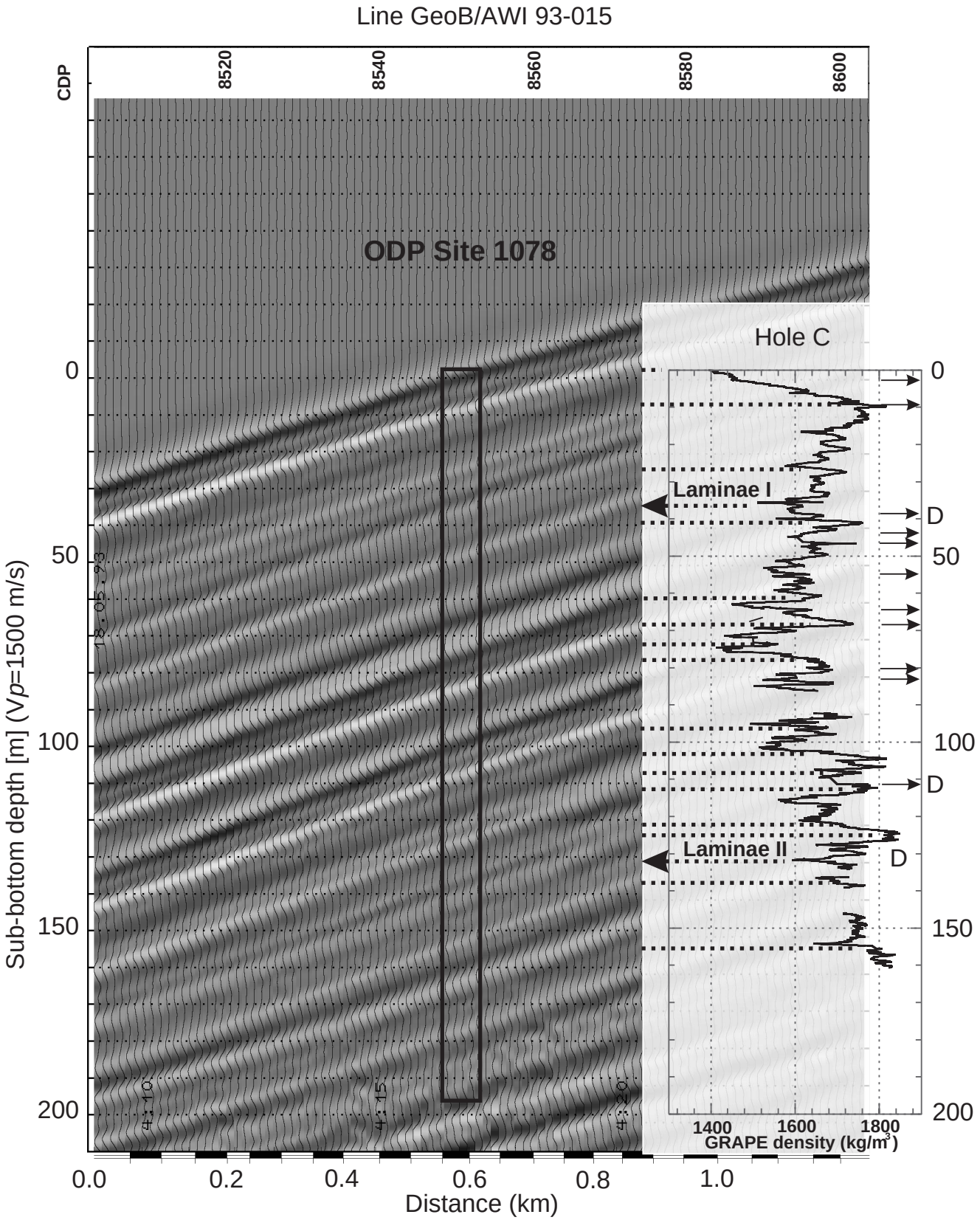

Figure 6. Close-up of Line GeoB/AWI 93-015 near Site 1078. Amplitudes are grayscaled. For comparison, wet bulk density data from index properties measurements are shown, and main reflectors are correlated with local extremes in the density log (thick dashed lines). For depth determination, a sound velocity (V_p) of 1500 m/s was used. Small arrows = extreme values in GRAPE density above 1800 kg/m^3; large arrows = laminated intervals; and D = descriptions of dolomitized layers in cores.

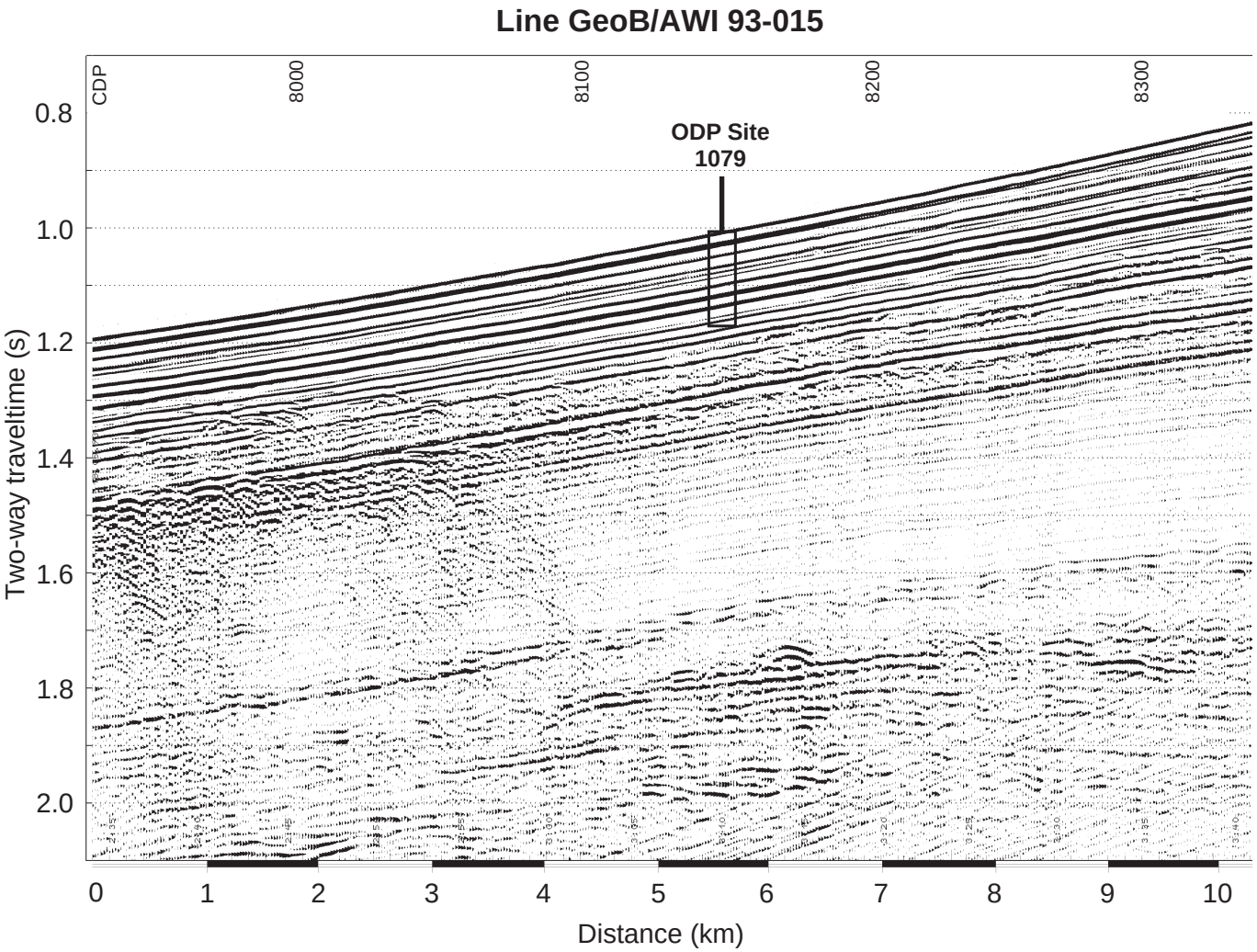

Figure 7. Seismic section of Line GeoB/AWI 93-015 at Site 1079. Vertical axis is given in two-way traveltime. CDP interval is 25 m for a shotpoint spacing of 25 m. Site 1079 is located at CDP 8150. The box indicates the approximate penetration of the borehole of 120 m.

Laminae are well preserved inside a 7-cm-thick dolomite concretion in the top of the laminated package in Section 175-1078C-15X-2 (Figs. 11, 13). The concretion is located within a transition into an overlying interval of nonlaminated sediments. It provides an opportunity to observe the bedding style of laminated sequences before significant compaction by sedimentary loading. Figure 11 shows that within the nodule, 1- to 2-mm-thick laminae are erosively truncated by a coarse silt layer 5 mm thick, suggesting that traction currents were important for forming at least some of the laminae.

Synthesis of Smear-Slide Analyses

Smear-slide analyses indicate that silty clay is the dominant lithology at Site 1078. The silt fraction is composed of subangular and angular mono- and polycrystalline quartz grains with subordinate amounts of feldspar. Both potassium and sodium feldspar are present. Muscovite, biotite, and detrital apatite are present in trace amounts. The biogenic component is represented by frequent foraminifer fragments and nannofossils. Diatoms are present in laminated sequences and in nonlaminated intervals, but they are absent in the nodule found in Section 175-1078C-15X-2. Laminated sequences also show abundant diatom resting spores. Trace amounts of plant remains and amorphous organic matter are occasionally observed. Secondary minerals include glauconite peloids that commonly contain euhedral pyrite grains indicating secondary consumption of iron to form pyrite. Examination of a smear slide made from scrapings of the dolomite concretion from the top of the laminated package in Section 175-1078C-15X-2 revealed that laminae within the concretion are composed of dolomite with rare, silt-sized subangular quartz grains and are barren of siliceous microfossils.

X-ray Diffraction Analysis

X-ray diffraction (XRD) analysis of sediments from Hole 1078A reveals that the clastic fraction is dominated by smectite, kaolinite and/or illite, quartz, the feldspar minerals albite and microcline, and muscovite. Pyrite is present as an accessory mineral in all samples. No clear identification could be made for other accessory phases. The smectites are generally poorly crystallized. Quartz and feldspar show comparable downcore variations (Fig. 14), which is probably caused by variations in grain size. In contrast to quartz, feldspar is not supplied by the Congo River (van der Gaast and Jansen, 1984). Feldspar originates from igneous complexes in southern Africa and therefore probably represents a southern sediment source fed by the Kunene River or by eolian dust. Consequently, the feldspar/quartz ratio may indicate the contribution of sediment supplied from the south.

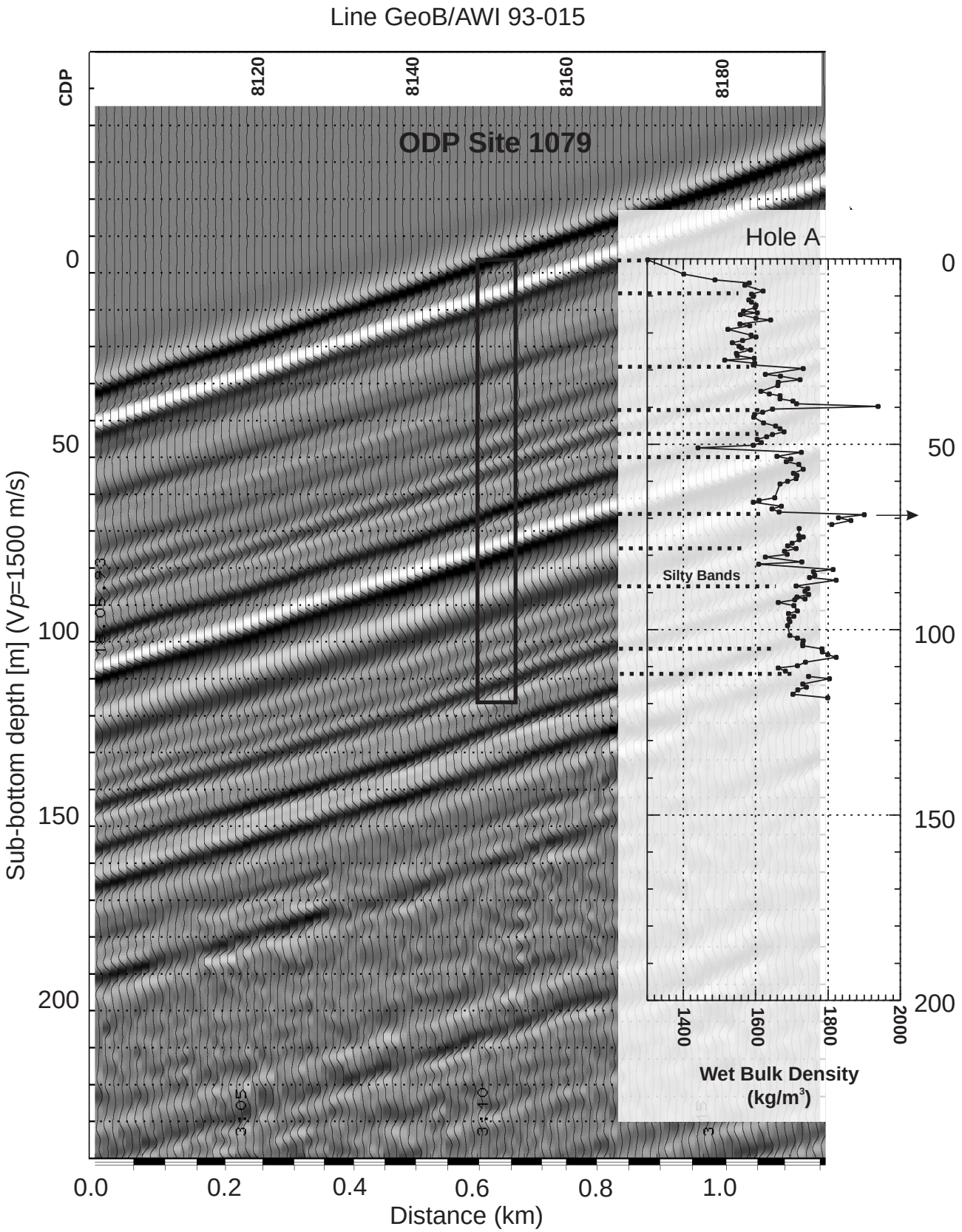

Figure 8. Close-up of Line GeoB/AWI 93-015 near Site 1079. Amplitudes are grayscaled. For comparison, wet bulk density data from index properties measurements are shown, and main reflectors are correlated with local extremes in the density log (thick dashed lines). For depth determination, a sound velocity (V_p) of 1500 m/s was used. Small arrow = extreme values in GRAPE density above 1800 kg/m^3.

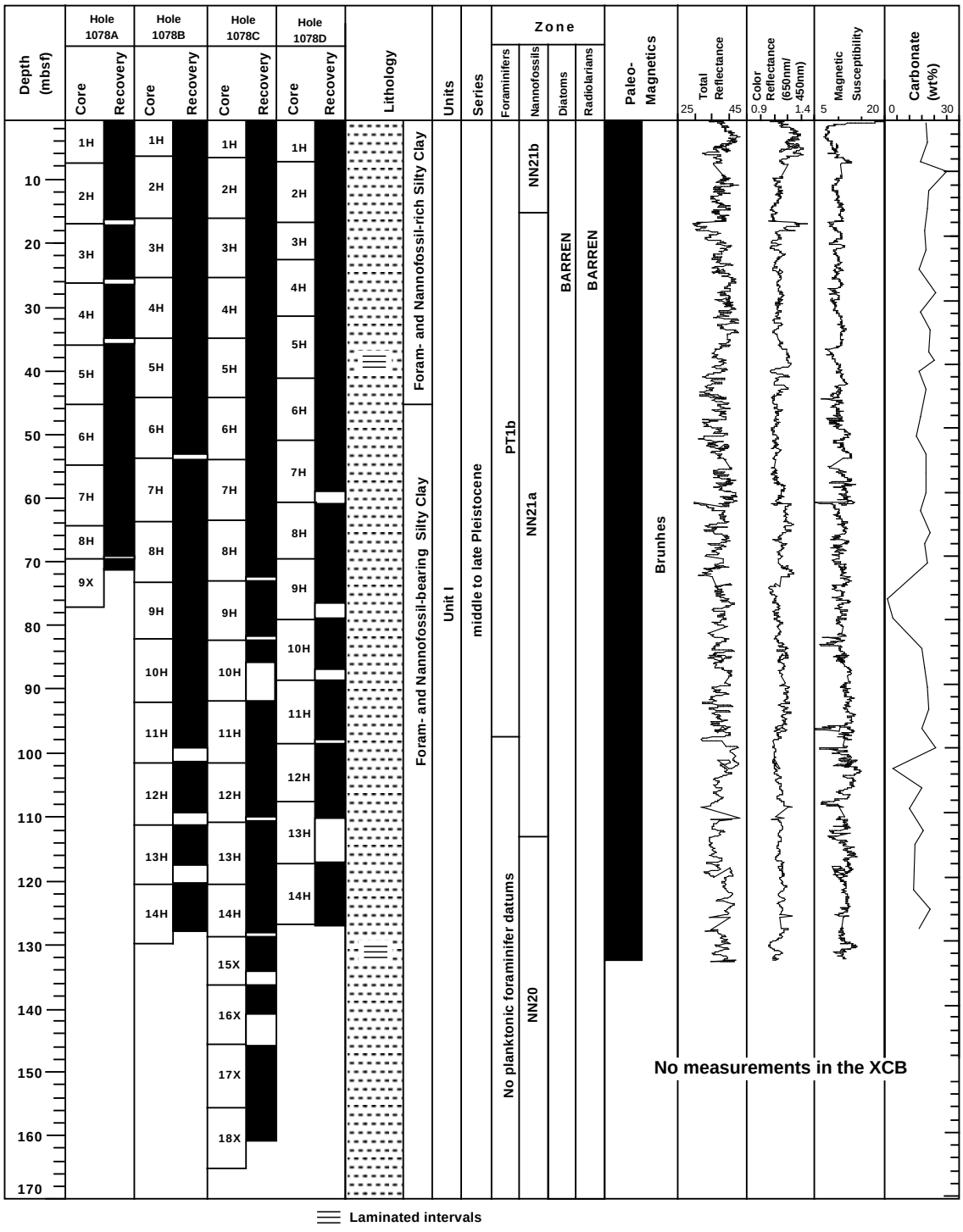

Figure 9. Composite stratigraphic section for Site 1078 showing core recovery at all holes, a simplified summary of lithology, age, total reflectance (400 – 700 nm), color reflectance (650 nm/450 nm), magnetic susceptibility, and calcium carbonate content.

Samples 175-1078B-9H-5, 46–47 cm, and 175-1078B-12H-1, 46–47 cm, were specifically analyzed by XRD to determine the mineralogy of the frequently present small whitish gray nodules. These two samples show the same mineral assemblage as other samples analyzed but have lower $CaCO_3$ contents. No additional accessory phases could be identified, suggesting that the whitish nodules are amorphous and/or are not sufficiently abundant to be detected by XRD.

Spectrophotometry

Color data were obtained at 2-cm intervals for Hole 1078A. Holes 1078B, 1078C, and 1078D were measured at 4-cm intervals. The reflectance values range between 30% and 45% throughout the column recovered from Site 1078. The total reflectance (Fig. 15) and red/blue (650 nm/450 nm) ratio (Fig. 16) data were smoothed over nine points for Hole 1078A and over five points for Holes 1078B, 1078C, and

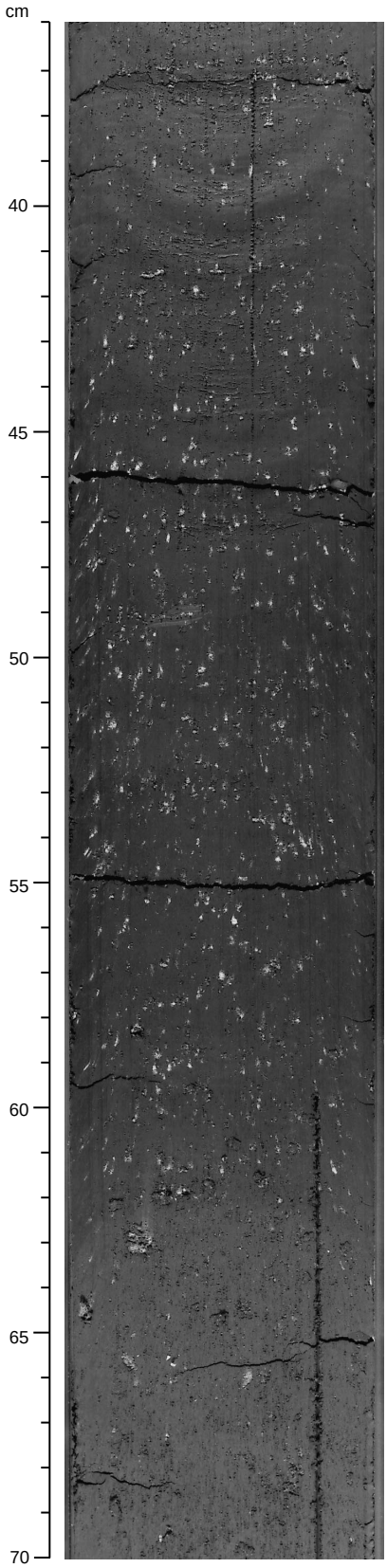

Figure 10. Photograph of disseminated whitish gray nodules in Section 175-1078-9H-5.

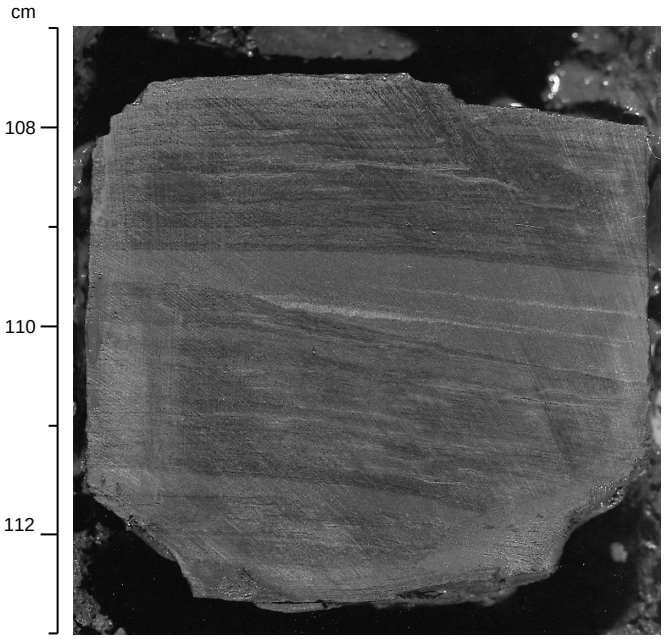

Figure 11. Close-up photograph of the dolomite horizon in the upper portion of the sequence of laminated sediments in Section 175-1078-15X-2. Note the erosive, lower contact of the 5-mm-thick coarse silt layer with the underlying laminae and the preserved burrow in the upper right. Cross-cutting relations indicate that bioturbation of the upper portion of the package of laminated sediments predated its cementation by authigenic dolomite.

1078D to remove smaller scale variability. Total reflectance shows the same trend in the four holes, although core disturbance caused by flow-in has been observed in several cores from Site 1078 (see above). Intervals with high and low reflectance spanning over 50 m are observed and according to the ages provided in the "Biostratigraphy and Sedimentation Rates" section (this chapter), could be related to interglacial cycles. The red/blue ratio shows a low variability downcore. Comparison between the total reflectance and the red/blue ratio with calcium carbonate content and the red/blue ratio with the organic carbon content shows no correlation (Fig. 17).

BIOSTRATIGRAPHY AND SEDIMENTATION RATES

Sediment recovered from Site 1078 represented a relatively continuous hemipelagic section spanning the last ~360 k.y. of the Pleistocene. The micropaleontological study was carried out on core-catcher samples. Additional samples from within the cores were examined for calcareous nannofossil biostratigraphy. Two laminated intervals were sampled at high resolution to examine their diatom content. With the exception of the laminated intervals, diatoms, silicoflagellates, and radiolarians are absent from this site. Calcareous microfossils are abundant and well preserved in all of the examined samples except for the laminated intervals, which are barren of nannofossils. Both calcareous nannofossils and planktonic foraminifers show evidence of reworking within the middle part of Hole 1078B.

Calcareous Nannofossils

Calcareous nannofossils were studied in core-catcher samples from Holes 1078A, 1078B, and 1078C. Additional samples from within cores of Holes 1078A and 1078B were examined to improve

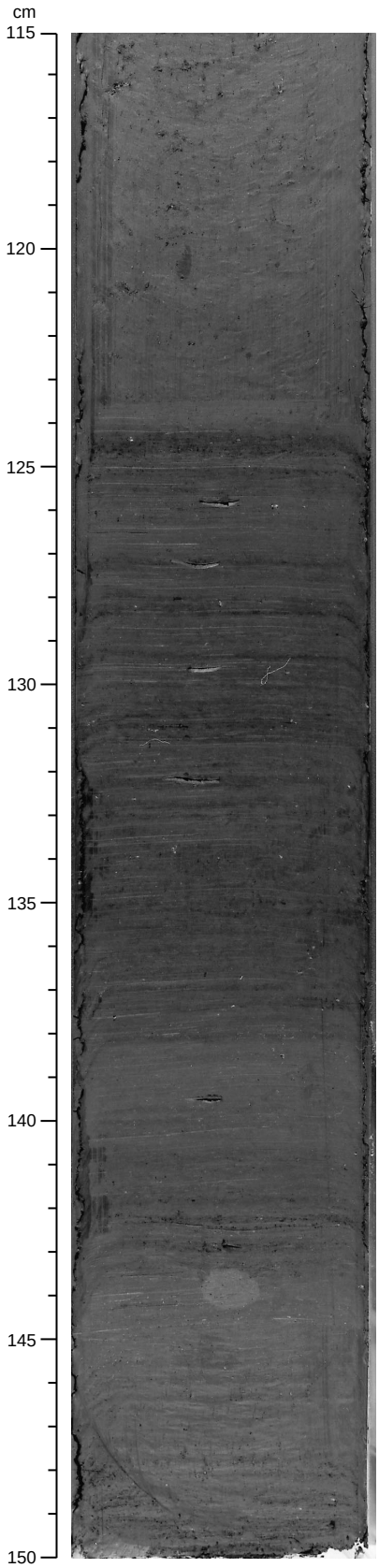

Figure 12. Photograph of the upper portion of the sequence of laminated sediments from Section 175-1078A-5H-2.

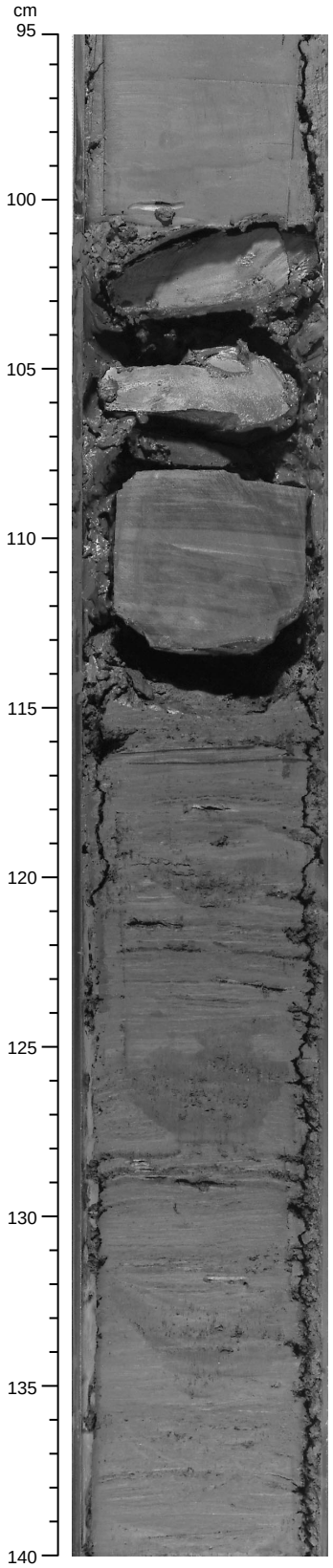

Figure 13. Photograph of the package of laminated sediments and authigenic dolomite horizon within its upper portion in Section 175-1078C-15X-2.

the biostratigraphic resolution. Preservation of nannofossil specimens is good to moderate. The overall abundance ranges from very abundant to abundant throughout the entire section of Site 1078, except within two short (~ 40-cm-long) laminated intervals (see "Diatoms," section, this chapter) in Cores 175-1078A-5H, 175-1078B-5H, 175-1078C-5H, and 175-1078C-15X, which are barren.

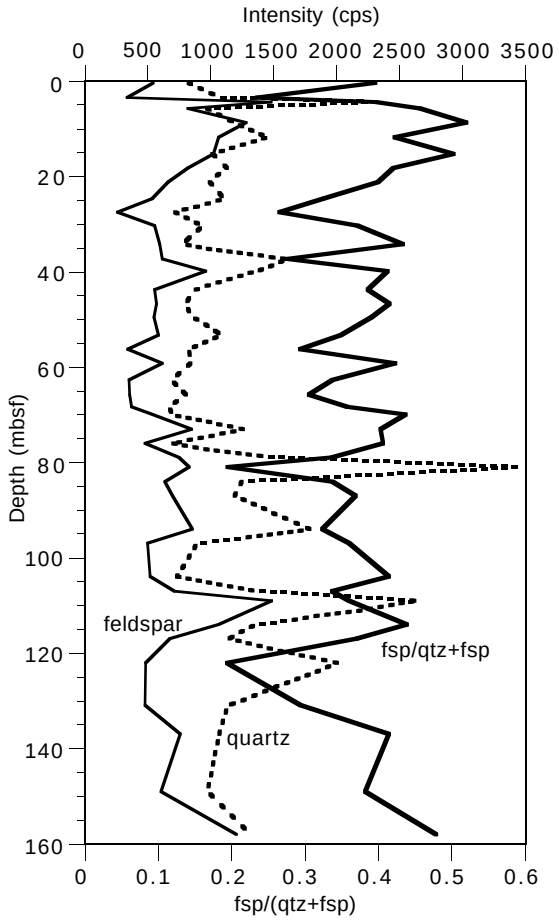

Figure 14. Stratigraphic variation in the ratio of feldspar to quartz, expressed as fsp/(qtz+fsp) and measured by XRD (cps = counts per second).

The nannofossil-based biostratigraphy (Table 2; Fig. 18) suggests that Site 1078 terminated within the upper half of Zone NN20, between 0.26 and ~0.36 Ma. The last occurrence (LO) of *Pseudoemiliania lacunosa*, the datum event for the Zone NN20/NN19 boundary (0.46 Ma), is not recognized in bottom samples of the deepest drilled Hole 1078C. Hole 1078A probably terminated close to 0.18 Ma, as predicted from applying the sedimentation rate pattern inferred from Holes 1078B and 1078C.

The stratigraphic record is rather continuous, except for two stratigraphically anomalous intervals. Sample 175-1078C-15X-CC, which is placed within Zone NN20 immediately below the Zone NN21a/NN20 boundary, is contaminated with abundant reworked flora of the Zone NN21a-aged interval. This core-catcher sample belongs to the top XCB core collected at Hole 1078C, therefore confirming the problem of contamination induced by the XCB coring device. Samples 175-1078B-9H-6, 120 cm, and 9H-CC contain a reworked nannofossil assemblage typical of Zone NN20 within the Zone NN21a part of the section. Both samples are part of an interval of highly disturbed material (see "Lithostratigraphy" section, this chapter). Oblique migration of older material through gas expansion could be one possible mechanism responsible for this stratigraphic anomaly.

Assuming a linear sedimentation rate between the two available datum events, sediments accumulated at a rate close to 60 cm/k.y. for the interval between 0.09 and 0.26 Ma (Zone NN21a).

Zone NN21b

The first occurrence of the *Emiliania huxleyi* acme which defines the Zone NN21b/NN21a boundary was recognized in all three investigated holes. The depth difference of this datum event between Hole 1078C and Holes 1078A and 1078B is essentially caused by low sampling resolution of Hole 1078C.

Zone NN21a

This stratigraphic interval spans most of the section of Site 1078. The LO of the *Gephyrocapsa caribbeanica* acme (Weaver, 1993), which marks the Zone NN21a/NN20 boundary, was identified both at Hole 1078B (Samples 175-1078B-12H-CC to 13H-6, 51–56 cm) and at Hole 1078C (Samples 175-1078C-13H-CC through 14H-CC).

Zone NN20

Drilling at Site 1078 recovered only the upper part of this zone.

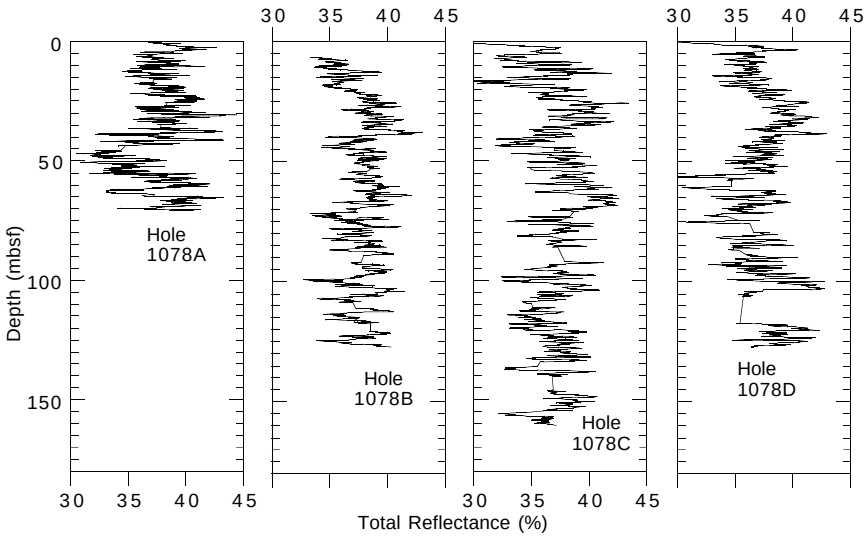

Figure 15. Stratigraphic variation in the total reflectance of visible light (400–700 nm) at Holes 1078A, 1078B, 1078C, and 1078D. A nine-point smoothing average was applied to the data set.

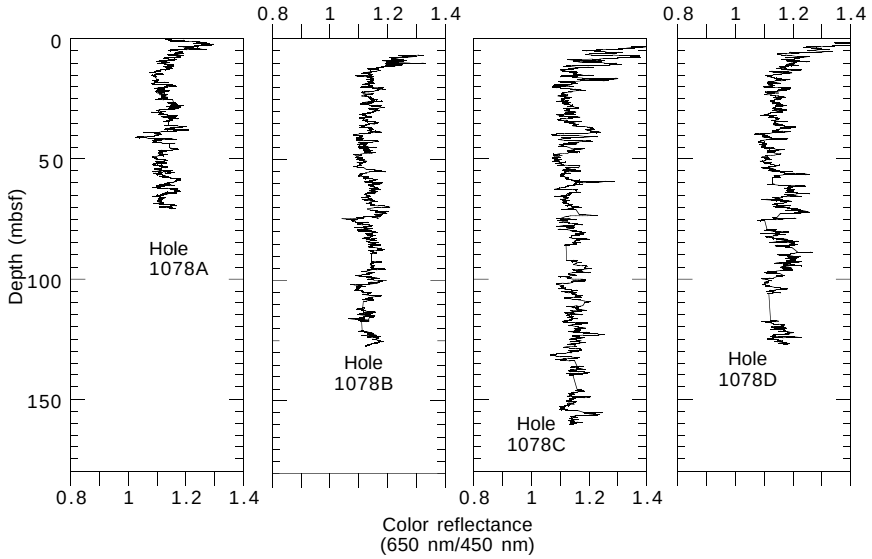

Figure 16. Stratigraphic variation in the ratio of the red (650 nm) to blue (450 nm) wavelengths at Holes 1078A, 1078B, 1078C, and 1078D. A five-point smoothing average was applied to the data set.

Planktonic Foraminifers

Core-catcher samples were analyzed from Cores 175-1078A-1H and 2H, Cores 175-1078B-2H through 14H, and Cores 175-1078C-15X through 18X. Planktonic foraminifers are common throughout the section, with the exception of Samples 175-1078B-12H-CC and 13H-CC, in which they are rare. Samples 175-1078C-16X-CC through 18X-CC contain only trace amounts of planktonic foraminifers.

The uppermost assemblage at Hole 1078A (7.4 mbsf) is dominated by high abundances of *Globigerinoides ruber* (pink), *Orbulina universa, Globigerina bulloides, Globigerinella siphonifera, Globigerinoides sacculifer*, and *Globorotalia inflata* (Table 3). Other species present but not abundant are *Globigerinoides ruber* (white), *Neogloboquadrina pachyderma* (dextral and sinistral), and *N. dutertrei* (Table 3).

Downcore faunal variations are based on analysis of Hole 1078B and suggest a change in surface-water conditions in Sample 175-1078B-12H-CC (Table 3). Below this level (109 mbsf), the fauna is dominated by *N. pachyderma* (Fig. 19). The high abundances of *N. pachyderma* in the lower part of the core may indicate a greater penetration of cool surface waters at that time (within Stage 8; i.e., when *N. pachyderma* is abundant, the Benguela Current penetrated the region). There is an overall increase in abundance of *G. ruber* above Sample 12H-CC (Table 3), which indicates that the system was dominated by warm surface water from Stage 8 and younger. The reduction in abundance of *N. pachyderma* may also indicate greater influence of a warmer surface water current such as the Angola Current, rather than an alteration in the position of the Benguela Current. It is possible that the dominance of *N. pachyderma* in the lower part of the section is the result of aliasing (i.e., because of the large sampling interval, only glacial periods were sampled below Sample 12H-CC and the interglacial above). Another factor to be considered is differential dissolution.

The two planktonic foraminiferal groups that provide biostratigraphic information for the Pleistocene, *G. tosaensis–G. truncatulinoides* and *G. tumida flexuosa*, are absent. Possibly, abundances of *G. inflata*, which has been used as a tracer of the Angola Benguela Front in this region (Jansen et al., 1996), could be used to erect a climatologic stratigraphy, based on more detailed postcruise work.

Benthic Foraminifers

Benthic foraminifers were analyzed from Holes 1078A, 1078B, and 1078C (partly) to obtain information on faunal changes through time (Table 4).

The benthic foraminiferal fauna at Site 1078 is well preserved and displays low diversity. The total abundance is very high, and the faunal assemblage is strongly dominated by *Bolivina* sp. 1 and *Bolivina* sp. 2. In all samples, except for the uppermost ones (Samples 175-1078A-1H-CC and 1H-CC through 2H-CC), these two species make up >50% of the total assemblage (~53%–99%). Additional species are *Cassidulina laevigata*, the *Praeglobobulimina/Globobulimina* group, and to some extent *Rectuvigerina* cf. *multicostata*. Besides high abundances of the mentioned species, the uppermost core catchers also exhibit high abundance of *Bolivina* sp. 1 (Sample 175-1078B-2H-CC, 27%) *Bulimina exilis* (Samples 175-1078A-1H-CC, 18%, and 175-1078B-1H-CC, 17%) and *Cancris auriculus* (Samples 175-1078A-1H-CC, 21% and 175-1078B-1H-CC, 4%). The species *Uvigerina peregrina* constitutes only 5% or less of the faunal assemblage, but in a few samples, this species becomes an important component (Samples 175-1078B-6H-CC, 21%; 175-1078C-14H-CC, 29%; and 175-1078C-17X-CC, 16%; Fig. 19).

The dominance of *Bolivina* sp. 1 and *Bolivina* sp. 2 and the overall low faunal diversity suggest low oxygen concentrations at the seafloor. *Bolivina* (and its close relatives *Suggrunda* and *Brizalina*) has been reported to be the most tolerant genus to low oxygen levels (Smith, 1963, 1964; Sellier de Civrieux and Bonilla, 1971; Phleger and Soutar, 1973). In a study of the Santa Barbara Basin, Phleger and Soutar (1973) found that although faunal diversity was low because of oxygen-depleted waters, the number of living individuals was larger than in nearby areas with higher oxygen concentrations. In oxygen-deficient areas off the western coast of South America, several studies have shown depletion in the benthic foraminiferal fauna along with a strong dominance of small-sized *Bolivina, Suggrunda*, and *Brizalina*, whose ornamentation was poorly developed (Sellier de Civrieux and Bonilla, 1971; Boltovskoy, 1972).

Diatoms and Radiolarians

Core-catcher samples from Holes 1078A, 1078B, and 1078C were analyzed for their diatom and radiolarian content. Samples were prepared as smear slides (for diatoms) and acid-cleaned (for both microfossil groups). The treated samples were washed with distilled water and sieved through 20-, 38-, or 63-µm sieves. Diatoms and radiolarians are absent in almost all core-catcher samples. Only a few diatoms and radiolarians are present in Sample 175-1078A-9X-CC. The presence of the radiolarian *Lamprocyrtis nigriniae* indicates a Quaternary age for Sample 175-1078A-9X-CC. Silicoflagellates are absent.

A laminated interval composed of alternating lighter olive and darker olive layers is seen in Core 175-1078A-5H, spanning Section

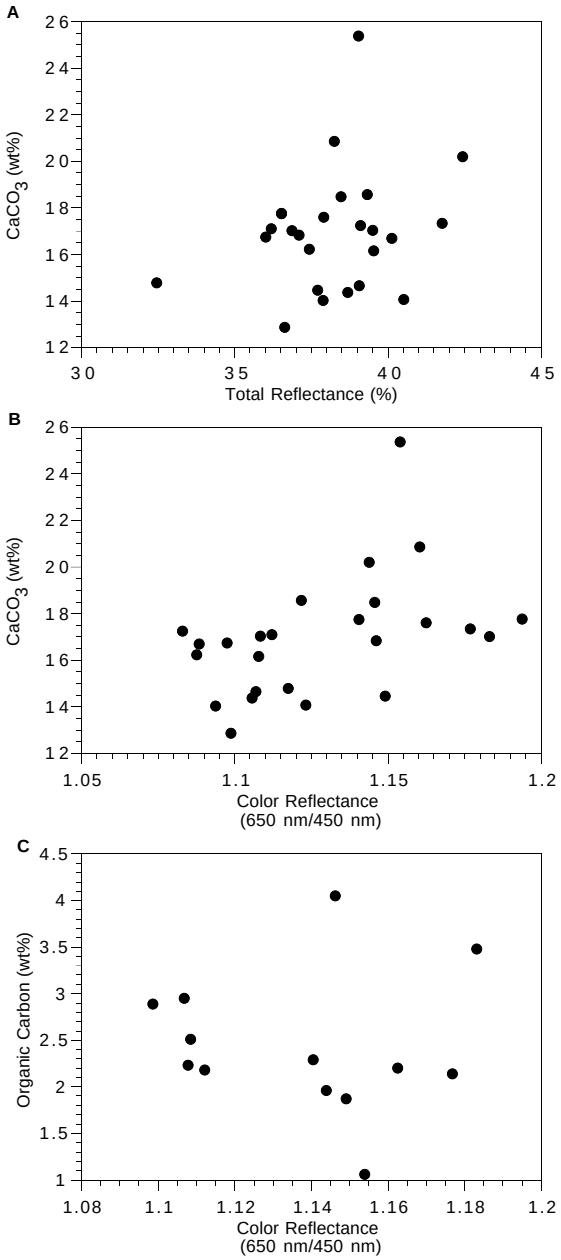

Figure 17. Comparison between (**A**) the total reflectance and calcium carbonate and between the red/blue wavelengths spectral ratio and concentrations of (**B**) calcium carbonate and (**C**) organic carbon at Hole 1078A.

5H-2, 124 cm, to 5H-3, 14 cm. This interval is also found at Hole 1078B (from Section 5H-3, 140 cm, to 5H-4, 30 cm), at Hole 1078C (from Section 5H-4, 10 cm, to 5H-4, 50 cm), and at Hole 1078D (from Section 5H-6, 14 cm, to 5H-6, 64 cm). These laminated intervals were sampled at high resolution, and smear slides were analyzed for their diatom content (Table 5). Diatom abundance ranges from common to rare; preservation is poor to moderate. The diatom assemblage is mixed and composed of the following:

1. A coastal upwelling flora characterized by *Chaetoceros* resting spores and *Thalassionema nitzschioides;*
2. An oceanic flora composed of taxa representative of oligotrophic conditions (e.g., *Azpeitia nodulifer, Rhizosolenia bergonii,* and *Alveus* (= *Nitzschia*) *marina*);
3. A neritic assemblage including *Paralia sulcata* and *Actinoptychus senarius;* and
4. A freshwater community characterized by *Cyclotella* spp.

Light and dark layers show similarity in species composition. The composition of the upwelling and freshwater flora is the same as that at Sites 1075, 1076, and 1077.

For radiolarians, a scrape sample from the laminated interval 175-1078B-5H-4, 0–30 cm, was taken. It contains common and well-preserved radiolarians. The assemblage is dominated by *Didymocyrtis tetrathalamus, Dictyocoryne* spp., *Octopyle stenozona, Tetrapyle octacantha,* and *Acanthodesmia vinculata,* indicating warm-water conditions. Upwelling species are present in low relative abundances. Silicoflagellates and *Actiniscus pentasterias* are also present.

A second laminated interval is seen in Section 175-1078C-15X-2, at 114–140 cm. Smear-slide analysis of light and dark layers indicate that the species content is similar to the one mentioned above, except that freshwater diatoms are absent (Table 5). Calcareous nannofossils are absent in both laminated intervals.

PALEOMAGNETISM

The investigation of magnetic properties at Site 1078 included the measurement of bulk susceptibility of whole-core sections and the natural remanent magnetization (NRM) of archive-half sections. The Tensor tool was used to orient Cores 175-1078A-3H through 8H, Cores 175-1078B-4H through 14H, and Cores 175-1078C-3H through 14H (Table 6). No cores from Hole 1078D were oriented.

Natural Remanent Magnetization and Magnetic Susceptibility

Measurements of NRM were made on all archive-half core sections from Holes 1078A, 1078B, 1078C, and 1078D, except those sections in which severe and pervasive core disturbance was visible. Sections from Hole 1078A were demagnetized by AF at 10 and 20

Table 2. Calcareous nannofossil datums at Holes 1078A, 1078B, and 1078C.

Event	Age (Ma)	Zone (base)		Core, section, interval (cm)		Depth (mbsf)		
		A	B	Top	Bottom	Top	Bottom	Mean
FO *Emiliania huxleyi* acme	0.09	NN21b		175-1078A-2H-5, 75	175-1078A-2H-CC	14.25	16.30	15.28
FO *Emiliania huxleyi* acme	0.09	NN21b		175-1078B-2H-5, 140	175-1078B-2H-CC	14.00	16.35	15.18
FO *Emiliania huxleyi*	0.26	NN21a	CN15	12H-CC	13H-6, 51-56	108.98	117.30	113.14
LO *Gephyrocapsa caribbeanica* acme	0.26	NN21a	CN15	12H-CC	13H-6, 51-56	108.98	117.30	113.14
FO *Emiliania huxleyi* acme	0.09	NN21b		175-1078C-2H-CC	175-1078C-3H-CC	16.48	26.29	21.39
FO *Emiliania huxleyi*	0.26	NN21a	CN15	13H-CC	14H-CC	121.68	128.79	125.24
LO *Gephyrocapsa caribbeanica* acme	0.26	NN21a	CN15	13H-CC	14H-CC	121.68	128.79	125.24

Notes: FO = first occurrence and LO = last occurrence. Zonal codes are those of (A) Martini (1971) and (B) Okada and Bukry (1980).

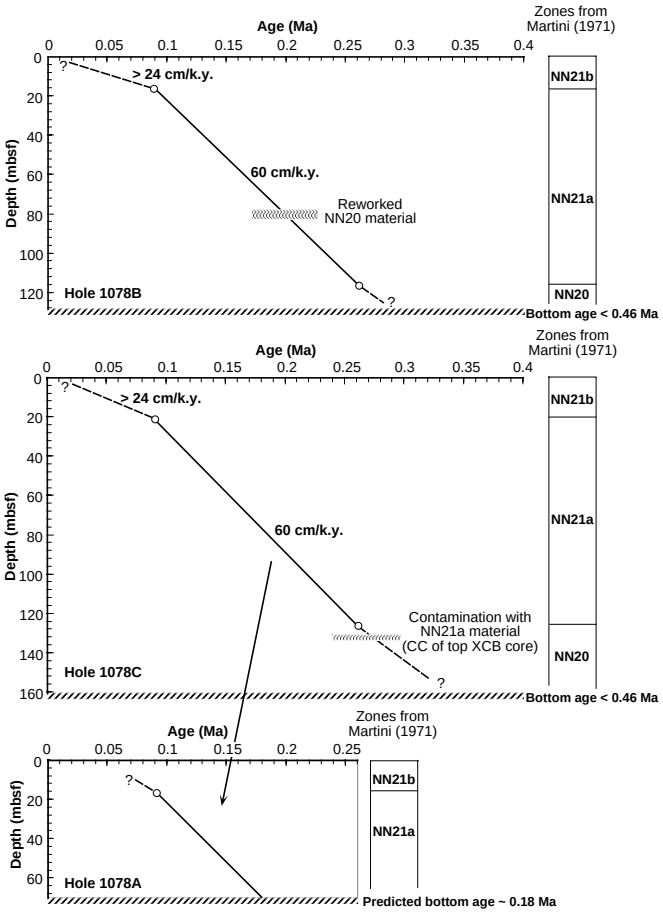

Figure 18. Age-depth plot and sedimentation rates estimated from calcareous nannofossil datums at Site 1078.

mT, and sections from Holes 1078B, 1078C, and 1078D were demagnetized by AF at 20 mT only.

Magnetic susceptibility measurements were made on whole cores from all four holes as part of the MST analysis (see "Physical Properties" section, this chapter). Magnetic susceptibility was relatively constant (between ~6 and 9×10^{-5} with depth (SI volume units; Fig. 20). The intensity of NRM after 20-mT demagnetization from the four holes is similar in magnitude, ranging generally from ~10^{-5} to ~10^{-3} A/m (Fig. 21, left panel). The NRM intensity shows fluctuations of more than an order of magnitude with depth, despite a relatively constant magnetic susceptibility.

A primary component of NRM is preserved in sediments from all four holes, except for the intervals where sediment flow-in occurred during core recovery. The magnetization of sediment flow-in shows steep positive inclinations after 20-mT demagnetization (Fig. 22). Before the cores were oriented using the Tensor tool data, the declinations were close to zero. This radial-inward direction (vertical upward from split surface of cores; positive-x in ODP archive coordinates) of the flow-in sediments was acquired in a magnetic field of the core barrel and cutting shoe. Some of the magnetic grains were possibly remobilized during sediment fluidization of the flow-in process and were re-aligned in the ambient magnetic-field direction. Roberts et al. (1996) also reported very steep inclinations acquired by flow-in sediments. Measurement of NRM proved to be a useful tool for detecting flow-in sediments in core sections, particularly in zones of uniform lithology where flow-in sediments are not physically apparent. At Site 1078, more than 10 possible flow-in zones were detected from the anomalous magnetization (marked "F" in Fig. 21). This remagnetization was particularly common at Hole 1078B, where it appeared in seven of 14 cores. Characteristics of the remagnetization associated with sediment flow-in, (the radial-inward and steep-downward direction, as well as coercivity >20 mT), are similar to the magnetic overprint acquired during the coring process (coring-induced magnetization [CIM]; see "Paleomagnetism" section, "Site 1077" chapter, this volume). This suggests that CIM is caused by partial remobilization of magnetic particles caused by penetration-generated shear stress. If this is true, neither AF nor thermal demagnetization will be able to remove the CIM because it could be carried by physically re-aligned single-domain and/or pseudo-single domain magnetic particles and thus have a coercivity spectrum similar to that of the primary component of postdepositional remanent magnetization.

Table 3. Dominant and abundant planktonic foraminiferal species at Holes 1078A, 1078B, and 1078C.

Core, section, interval	Depth (mbsf)	Abundance	*Globigerinoides ruber* (pink)	*Globigerinoides ruber*	*Orbulina universa*	*Globigerinoides sacculifer*	*Globigerina bulloides*	*Globigerinella siphonifera*	*Globorotalia inflata*	*Globorotalia menardii*	*Neogloboquadrina dutertrei*	*Neogloboquadrina pachyderma* (dextral)	*Neogloboquadrina pachyderma* (sinistral)	*Globorotalia crassaformis*
175-1078A-														
1H-CC	7.4		A		A		A	A	A					
2H-CC	16.3		A				A		A				A	
175-1078B-														
2H-CC	16.4			A	A				D			A		
3H-CC	26.0		A		D		D							
4H-CC	35.6		A	A	A	A	A							
5H-CC	45.3		A	A	D	A								
6H-CC	53.6		A	D	A									
7H-CC	64.9		A	A	A									
8H-CC	74.8			A	D				A					
9H-CC	83.2			A	D							A		
10H-CC	89.5			A	D		A		A					
11H-CC	102.0			A	A	A			A					
12H-CC	109.0	R												
13H-CC	117.3	R												
14H-CC	127.9		A	A	A							A		A
175-1078C-														
15X-CC	134.4				D				A			A	A	
16X-CC	140.3	T			D									
17X-CC	155.4	T										A		
18X-CC	160.9	T			D							D		

Notes: D = dominant (>30%); A = abundant (10%–30%); R = rare (1%–5%); and T = trace (<1%).

Magnetostratigraphy

We identified the polarity of the NRM from the declination and inclination. Inclinations and declinations from all four holes indicate that only the Brunhes (C1n) normal polarity Chron (Berggren et al., 1995) is recorded in these sediments (an inclination of –23° is expected from the geocentric axial dipole model; see Fig. 21, middle and right panels). In spite of the high sedimentation rate, based on biostratigraphy, short reversal events and/or excursions in the Brunhes Chron (such as the Blake event) were not found. Anomalous directions seen in Figure 21 were caused by the sediment flow-in discussed above or by other physical disturbance of the cores.

COMPOSITE SECTION

Measurements from the MST of magnetic susceptibility and GRAPE density, sampled at 2- to 4-cm intervals, and color reflectance, discretely measured at 2- to 4-cm resolution, were used to es-

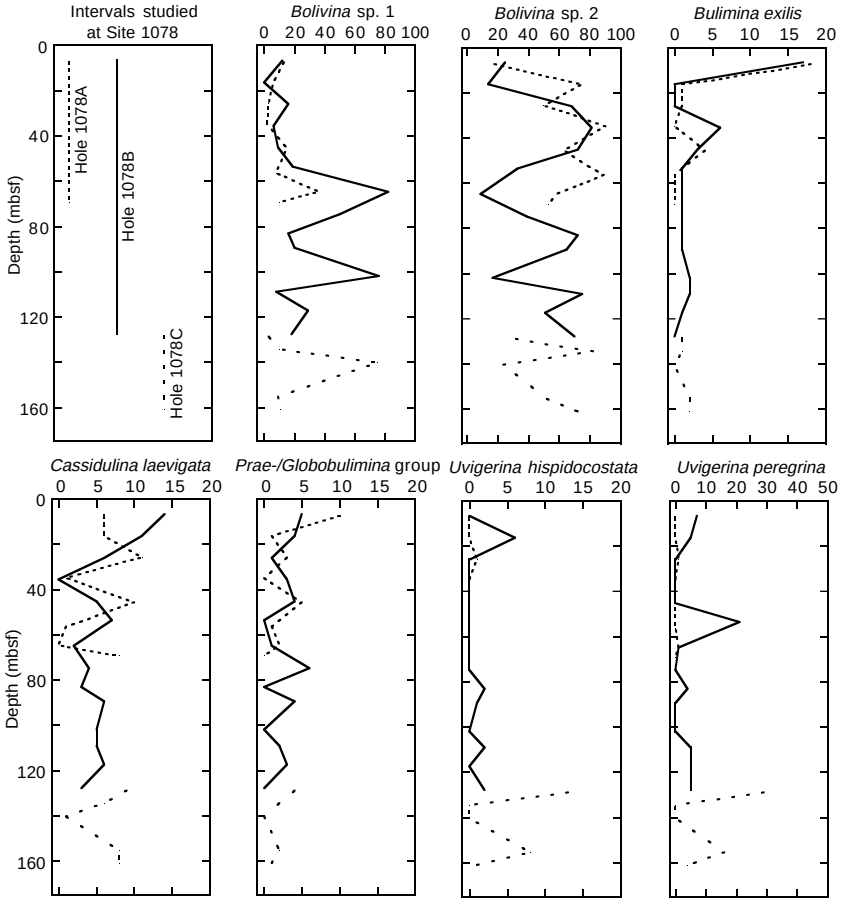

Figure 19. Relative abundances (in percentages) of selected benthic foraminiferal species at Holes 1078A, 1078B, and 1078C.

tablish interhole depth continuity at Site 1078. Sedimentary features in the MST and color reflectance data of adjacent holes were graphically and quantitatively adjusted to be at approximately the same relative depth, thus generating a composite depth scale (expressed as meters composite depth [mcd]). Working from the core top down, a constant is added to the meters below seafloor (mbsf) scale of each core to establish the mcd depth offsets for individual cores. Establishing continuity of the Site 1078 stratigraphic sequence was problematic because of insufficient intercore overlap of the first three cores and intervals of high scatter in the data. However, a composite section was documented between 16 and 91 mcd.

Magnetic susceptibility, GRAPE, and color reflectance (red/blue ratio [650 nm/450 nm] and chromaticity b*) data were all used to construct a composite section and to verify core gaps. Because of the presence of gas voids and scatter in the data, no single parameter was uniformly reliable through the entire hole to constrain intercore correlation; thus, all parameters were used where appropriate. In addition, core flow-in was identified in the bottom section(s) of a number of cores, particularly those at Hole 1078B (see "Lithostratigraphy" and "Paleomagnetism" sections, this chapter, for further discussion). Disturbed sections were avoided when correlating between cores. To reduce the scatter in the raw MST measurements, raw data were filtered. Details of the filtering process are documented in the "Composite Section" section, "Site 1075" chapter (this volume), with the exception that a nine-point Gaussian filter was used to smooth the color reflectance data, and a six-point Gaussian smoothing was used for the GRAPE data.

Continuity of the composite section record is documented between 16 and 91 mcd (Fig. 23; Table 7). Composite splices used to constrain core gaps ranged from fair to very good. Lack of overlap among Holes at Site 1078 at 7 and 16 mbsf precluded the determination of core gaps among the three top cores. Between 16 and 57 mcd, the composite section is very good; however, the magnetic susceptibility and GRAPE display high scatter between 42 and 52 mcd, which made us shift reliance to color reflectance data for constraining the splice over this interval. The postulated overlap at ~57 m should be regarded with caution. The splice relies on a small positive feature observed in color reflectance (chromaticity b* and red/blue ratio) in both Sections 175-1078A-6H-7 and 175-1078C-7H-1. The correlation is not supported by the GRAPE and magnetic susceptibility records. Below 57 m, generally high scatter in the data degrade the quality and confidence of the spliced intervals. Despite these caveats, there is good agreement found in establishing a composite section to 91 mcd. The growth of the mcd scale relative to the mbsf scale was ~7% (Fig. 24)

Upon completion of the composite depth sections, a single spliced record was assembled using overlapping cores from Holes 1078A, 1078B, 1078C, and 1078D for GRAPE, magnetic susceptibility, and color reflectance (red/blue ratio [650 nm/450 nm]; Fig. 25). Hole 1078C served as the backbone for the sampling splice. Adjacent holes, primarily 1078D, were used to splice across core gaps in the Hole 1078C sequence. Intervals of core flow-in and disturbance were avoided, where possible, in assembling the splice. The splice for Site 1078 (Table 8) can be used as a sampling guide.

INORGANIC GEOCHEMISTRY

Sixteen interstitial water samples were collected at Holes 1078A, 1078B, and 1078C over a depth range from 1.4 to 150.3 mbsf (Table 9) to provide information about diagenetic reactions occurring in the Angola Basin. In addition to the changes in interstitial water composition caused by organic carbon degradation, carbonate dissolution and reprecipitation, and other chemical reactions, the strong decrease in sedimentation rate from ~60 cm/k.y. at depths below ~15 mbsf to much lower values in the uppermost sequence (>24 cm/k.y.; see

Table 4. Relative abundance of benthic foraminiferal species and overall abundance of benthic foraminifers at Holes 1078A, 1078B, and 1078C.

Core, section, interval	Depth (mbsf)	Abundance	*Bolivina ordinaria*	*Bolivina* sp. 1	*Bolivina* sp. 2	*Bolivina* sp. 3	*Bolivina spathulata*	*Bulimina aculeata*	*Bulimina exilis*	*Bulimina marginata*	*Bulimina mexicana*	*Bulimina* sp.1	*Cancris auriculus*	*Cassidulina laevigata*	*Cassidulinoides* cf. *bradyi*	*Chilostomella oolina*	*Chilostomella ovoidea*	*Cibicidoides pachyderma*	*Discorbinella bertheloti*	*Ehrenbergina trigona*	*Epistominella* sp. 1	*Fursenkoina* sp. 1	*Hoeglundina elegans*	*Hyalinea balthica*	*Lenticulina* sp. 1	*Martinottiella communis*	*Nodosaria* spp.	*Nonionella turgida*	*Oolina* spp.	*Oridorsalis umbonatus*	*Planulina* sp. 3	*Praeglobobulimina/Globobulimina* group	*Pullenia subcarinata*	*Pyrgo* spp.	*Quadrimorphina allomorphinoides*	*Quinqueloculina* spp.	*Rectuvigerina* cf. *multicostata*	*Sigmoilinopsis schlumbergeri*	*Siphotextularia catenata*	*Sphaeroidina bulloides*	*Spiroloculina* sp. 1	*Uvigerina auberiana*	*Uvigerina hispidocostata*	*Uvigerina peregrina*	Unidentified	Number of specimens counted
175-1078A-																																													
1H-CC	7.40	A	1	13	18				18				21	6			+					3									10					9										271
2H-CC	16.30	A		6	75				1					6			+				10										+			+		+									416
3H-CC	25.83	A		3	50	+		+	+		+	+	+	11	3		+		+	1	6	+	+	6	+	+	+	+	+	+	3	+		+	+	3	+	+	+	+		1	+	3	724
4H-CC	34.87	A		2	90									+							6			1						+														279
5H-CC	45.59	A		15	63	+			4				+	10					+									+			5														240
6H-CC	56.39	A		8	89				+					1			+											+			+														393
7H-CC	64.69	A		36	59	+				+			+	+																+	2				+							+	+		792
8H-CC	69.32	A		10	53	1				5		5	1	8			1								+					1	4					2								8	449
175-1078B-																																														
1H-CC	6.61	A		12	25	4			17				4	14			2				+							+		+	5					8						+	7	2	415
2H-CC	16.35	A		+	14	27						+		11		1	5				2			+	+			+	+	+	4		+		+	6	10	+			1	6	5	2	438
3H-CC	26.00	A		16	68	+			+				+	6	1						4			2						1														474
4H-CC	35.61	A		6	81	+			6				+																		3					3									310
5H-CC	45.25	A		9	72				3				2	5	+																4				+	3									311
6H-CC	53.56	A		19	33	1		1	1	6		1	+	7			+							+		+		+		+	6	+				+							21		283
7H-CC	64.86	A		82	9	+		1	+			+	+	2														+		+	2	+											1		358
8H-CC	74.77	A		50	39				+					4																	6														239
9H-CC	83.15	A		16	72	+			+				+	3																	2	+				+		+				2	4		552
10H-CC	89.49	A		20	65	+		+	+			+		6			+														+	4						+				+	+		383
11H-CC	101.98	A		76	17				2					5																															327
12H-CC	108.98	A		8	75				2					5				+										+		+		2											2	5		322
13H-CC	117.30	A		29	51				1		1		+	6			+														+	3					2							5		354
14H-CC	127.85	A		18	70						+		+	3											+						+					1						2	5		309
175-1078C-																																														
14H-CC	128.79	A		3	32				+			3	+	9														+		+	1	4	+		+		+		+				13	29	1	344
15X-CC	134.36	A		10	82				+					6																	2														307
16X-CC	140.33	A		75	24									+																	+													+	328
17X-CC	155.37	A		9	52				2	3			+	8																+	2												8	16		258
18X-CC	160.94	A		11	72				2					8							+										1					1								1	4		281

Notes: The relative abundance of benthic foraminiferal species is given as a percentage, where + = <1%. Absolute abundance (per ~20 cm^3 of sediment) of benthic foraminifers is given as A = abundant (>500 specimens); C = common (250–500 specimens); F = few (100–249 specimens); R = rare (50–99 specimens); T = trace (1–49 specimens); and B = barren (no specimens).

"Biostratigraphy and Sedimentation Rates" section, this chapter) has a profound effect on the diagenetic reactions occurring at Site 1078. On all profiles, the chemical distributions at Site 1077, which are broadly representative of the sites drilled in the Congo Basin, are provided for interbasinal comparison purposes.

Alkalinity, Sulfate, and Ammonium

Downcore profiles of alkalinity, sulfate, and ammonium (Fig. 26) reflect the degradation of organic matter, as has been observed at Sites 1075, 1076, and 1077. Of particular interest at Site 1078, however, is the influence of the change in sedimentation rate at ~15 mbsf. Below this depth, there is a marked change in slope in the alkalinity gradient, and sulfate has been almost completely consumed. These profiles show the effect of the decrease in sedimentation rate through time; below 15 mbsf, where sedimentation occurred more rapidly, faster burial of organic matter resulted in complete depletion of sulfate and the accumulation of alkalinity, whereas above 15 mbsf the chemical profiles are dominated by diffusion from seawater. Thus, the 15-mbsf depth is a profound boundary at Site 1078, as will be seen in other profiles as well.

Dissolved ammonium increases monotonously to maximum values at 60–70 mbsf and remains constant from that depth to the bottom of Hole 1078C. These concentrations are very high compared with those documented at the Congo Basin. The clear change in behavior of the distribution of ammonium at 75 mbsf does not correspond to a horizon or depth interval of particular interest of which we are aware, and its cause at this point remains unknown.

Table 5. Diatom abundance and assemblage composition within two laminated intervals at Holes 1078A and 1078C.

Core, section, interval (cm)	Depth (mbsf)	Overall abundance	Lamina color	Upwelling	Neritic	Open-ocean	Freshwater	Silicoflagellates
175-1078A-								
5H-2, 126.0	38.79	R	Light	T		T	T	
5H-2, 127.5	38.81	R	Dark		T	T		
5H-2, 129.5	38.83	R-F	Light	T	T	T	T	
5H-2, 132.0	38.85	R	Dark		T	T	T	
5H-2, 139.5	38.93	R	Light	T	T	T	T	T
5H-2, 143.0	38.96	R	Dark	T	T	T	T	
5H-3, 4.0	39.07	F	Light	T	T	T	T	T
5H-3, 70	39.73	F	Dark	C	T	T	T	
175-1078C-								
15X-2, 120.7	131.51	R	Dark	T		R		
15X-2, 122.6	131.53	F	Dark	F	T	T		T
15X-2, 128.2	131.58	C	Light	A		T		T
15X-2, 131.5	131.62	R	Light	T	T	T		T

Note: R = rare; F = few; C = common; T = trace; and A = abundant.

Table 6. Tensor tool–orientation data for cores from Holes 1078A, 1078B, and 1078C.

Core, section	MTF (°)	Inclination angle
175-1078A-		
3H	5	1.26
4H	144	1.12
5H	63	1.09
6H	3	0.89
7H	131	0.66
8H	305	0.67
175-1078B-		
4H	31	0.49
5H	117	0.22
6H	143	0.58
7H	74	0.67
8H	323	0.94
9H	232	0.84
10H	69	1.17
11H	174	0.91
12H	16	1.11
13H	202	0.97
14H	272	1.22
175-1078C-		
3H	126	0.37
4H	129	0.45
5H	263	0.65
6H	133	0.60
7H	277	0.64
8H	160	0.50
9H	300	0.42
10H	165	0.36
11H	156	0.40
12H	353	0.54
13H	74	0.36
14H	83	0.29

Notes: The orientation parameter (MTF) is the angle in degrees between magnetic north and the double line marked on the center of the working half of the core. The local declination anomaly is 9°W.

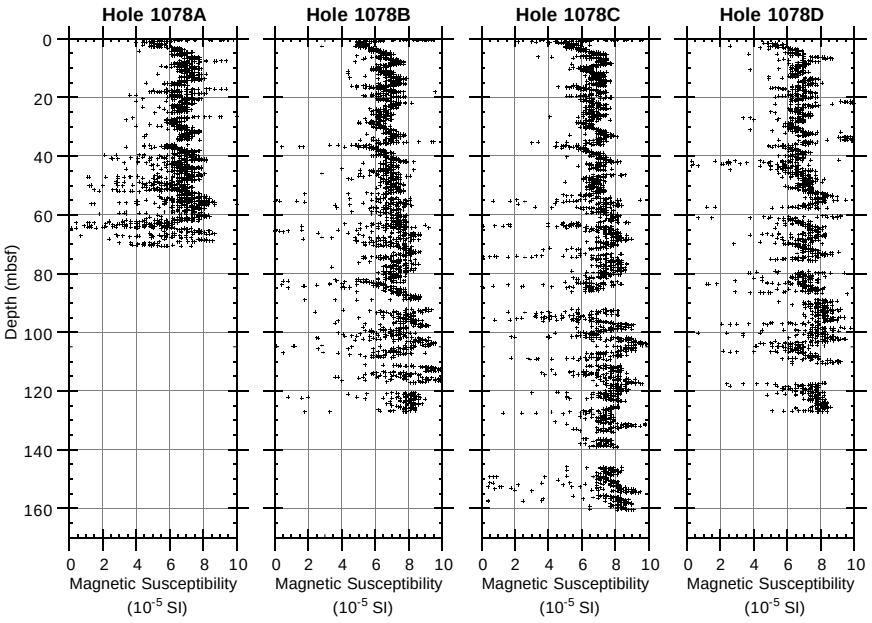

Figure 20. Magnetic susceptibility from MST data (volume corrected) for Holes 1078A, 1078B, 1078C, and 1078D.

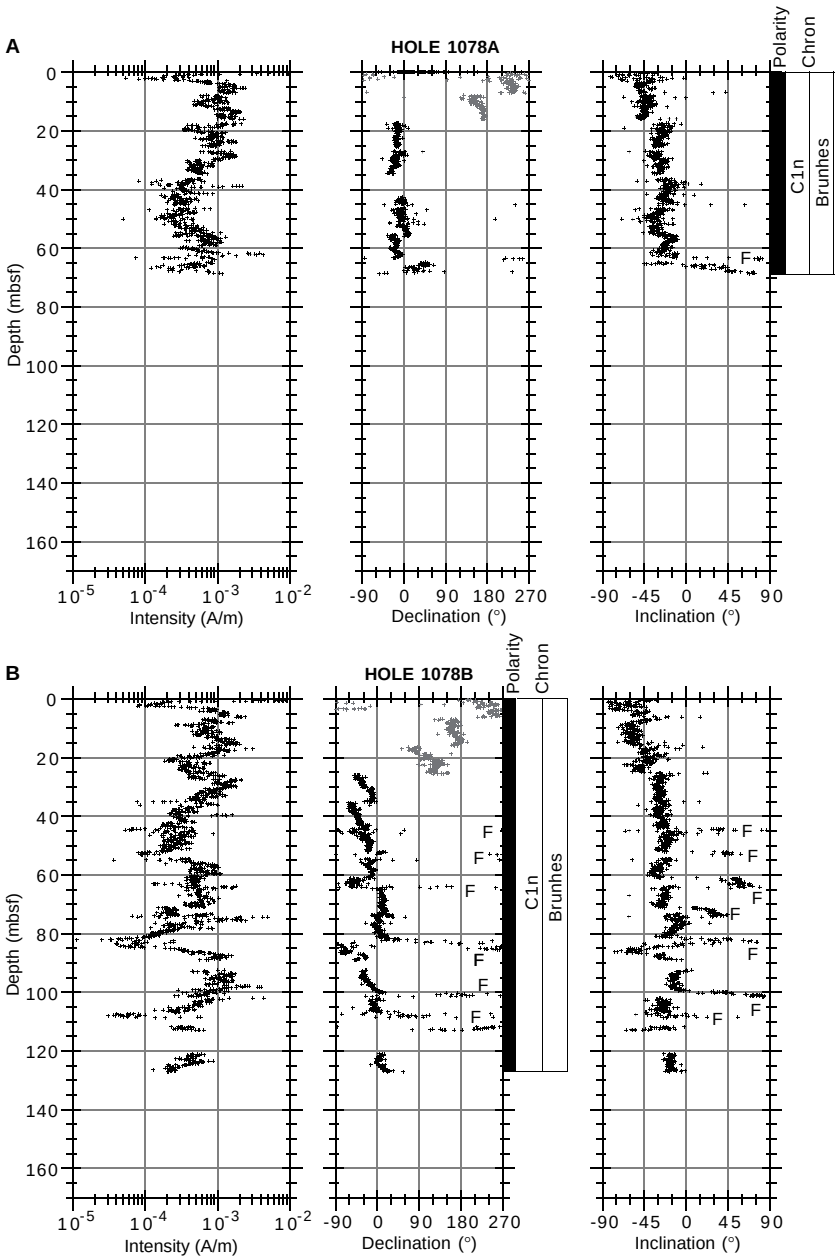

Figure 21. NRM intensity, declination, inclination, and magnetostratigraphic interpretation after 20-mT demagnetization. Black symbols = Tensor corrected; gray symbols = uncorrected; F = sediment flow-in. Polarity shading: black = normal. **A.** Hole 1078A. **B.** Hole 1078B. (Continued on next page.)

Calcium, Magnesium, and Strontium

The effect of the change in sedimentation rate at 15 mbsf is also observed in the profiles of elements that respond to carbonate dissolution and reprecipitation, such as Ca^{2+}, Mg^{2+}, and Sr^{2+} (Fig. 27). Through the 0–15 mbsf depth range, Ca^{2+} concentrations decrease by 6 mM, whereas Mg^{2+} concentrations decrease by 3 mM and Sr^{2+} by 26 µM. Because there is a greater molar decrease in Ca^{2+} than in Mg^{2+} and there is an associated decrease in Sr^{2+}, the process of Ca^{2+} dissolution (release of Sr^{2+}) and dolomite precipitation (decrease in Ca^{2+} and Mg^{2+}) cannot be solely responsible, and an additional sink for both the Ca^{2+} and Sr^{2+} must exist. We postulate that this sink is finely disseminated diagenetic apatite. Small amounts of diagenetic apatite that would be undetectable by XRD could cause the simultaneous decrease in Ca^{2+} and Sr^{2+} while not affecting the phosphate profile (which will be dominated by the source provided by organic matter degradation, as discussed below). Regardless of which phase(s) is involved in the consumption of dissolved Ca^{2+} and Sr^{2+}, its precipitation is essentially confined to the uppermost 15 mbsf.

Below this depth, Ca^{2+} concentrations remain essentially constant, Mg^{2+} concentrations decrease (perhaps recording uptake by clays), whereas Sr^{2+} stays essentially constant (with noise) after an increase from 10 to 40 mbsf.

Silica and Phosphate

Dissolved silica increases in concentration very rapidly through the uppermost 5–6 m of sediment (Fig. 28), recording the dissolution of biogenic opal. Below a minor maximum at ~40 mbsf, concentrations decrease slightly, most likely recording authigenic clay mineral formation. The concentrations of dissolved silica are lower than at Site 1077, reflecting the generally low abundances of diatoms in this sequence (see "Biostratigraphy and Sedimentation Rates" section, this chapter).

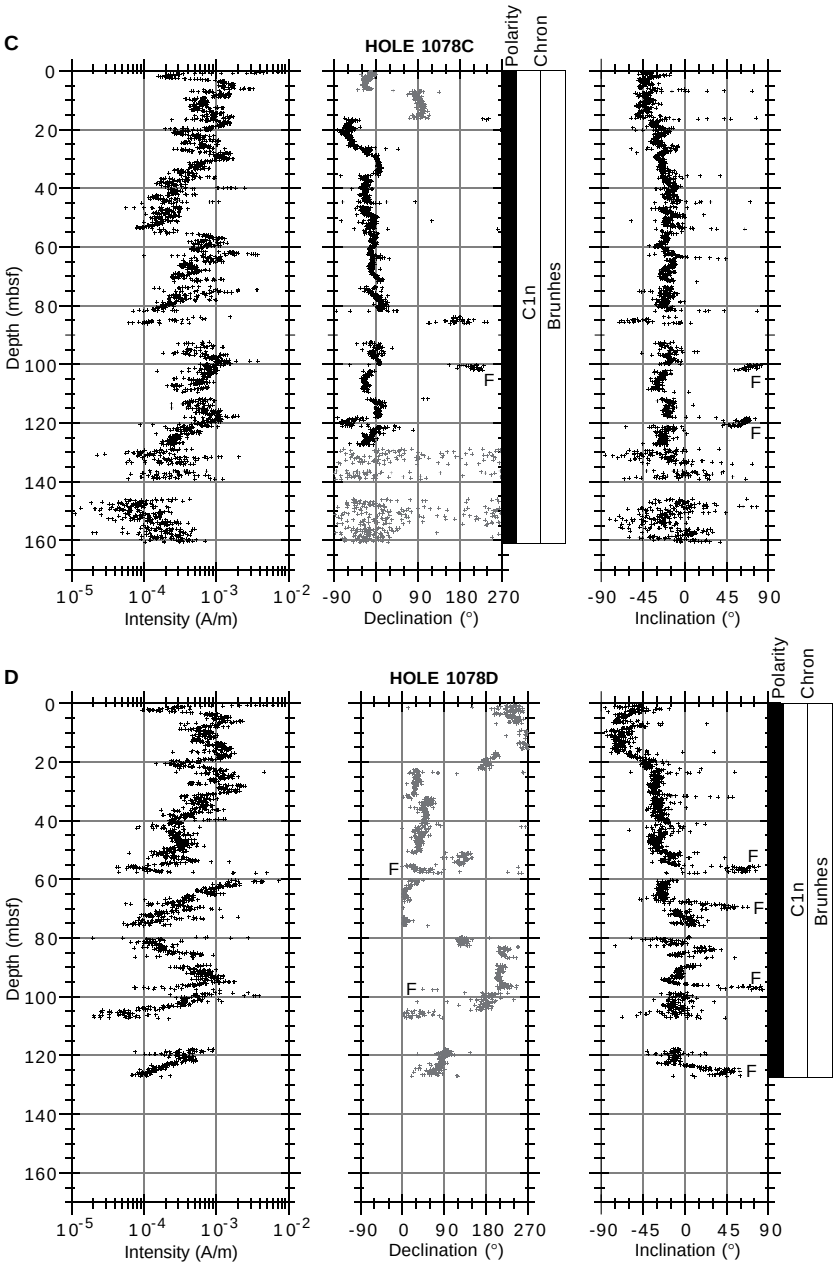

Figure 21 (continued). **C.** Hole 1078C. **D**. Hole 1078D.

Dissolved phosphate increases very rapidly to a maximum value of ~150 µM within the uppermost 15 mbsf. This increase, which occurs through the same depth range as the increase in alkalinity and the consumption of sulfate is caused by degradation of organic matter. If authigenic apatite is forming through this depth interval, as hypothesized above, the consumption of dissolved phosphate by such authigenesis is much less than its production during organic destruction.

Sodium and Potassium

Concentrations of dissolved Na^+ steadily increase with depth downcore (Fig. 29), most likely reflecting cation exchange reactions involved with authigenic clay formation. Compared with Site 1077 in the Congo Basin, however, the release of Na^+ is much greater, which potentially reflects contrasts in detrital mineralogy. The profile of dissolved K^+ decreases through the uppermost 15 mbsf, before increasing with depth. The reasons behind the K^+ decrease in the uppermost 15 mbsf remain unknown. Although K^+ is commonly associated with clay exchange reactions along with Na^+, based on the shipboard data we are unable to interpret the K^+ decrease occurring in the uppermost 15 mbsf within the context of the other reactions, discussed above.

Salinity and Chloride

The profiles of salinity and Cl^- also show marked gradients in the uppermost 15 mbsf (Fig. 30). Salinity values decrease, which most likely reflects the strong removal of sulfate over the same depth range, before increasing to a maximum value of 36 at 70 mbsf. Below 15 mbsf, the profile of salinity closely follows that of ammonium. Dissolved Cl^-, however, increases through the upper 15 mbsf before decreasing to minimum values at depth. It is unclear at this point whether the initial increase in Cl^- is caused by a glacial ice volume signal, as we hypothesize is the case for the distributions at Site 1075,

or is related to diagenetic processes operating through this portion of the sedimentary succession.

ORGANIC GEOCHEMISTRY

Calcium carbonate and organic carbon concentrations were measured on sediment samples from Site 1078 (Table 10). Organic matter atomic carbon/nitrogen (C/N) ratios and Rock-Eval pyrolysis analyses were employed to determine the type of organic matter contained within the sediments. High gas contents were encountered, and routine monitoring of the sedimentary gases was done for drilling safety.

Inorganic and Organic Carbon Concentrations

Concentrations of carbonate carbon are low in Site 1078 sediments. They vary between 3.0 and 1.3 wt% (Table 10). The maximum carbonate carbon concentration is equivalent to 25.4 wt% sedimentary $CaCO_3$. These moderately low concentrations agree with the low abundances of coccoliths and other calcareous microfossils in these hemipelagic sediments (see "Biostratigraphy and Sedimentation Rates" section, this chapter). The range in concentrations reflects a varying combination of changes in biological production of calcareous material, dilution by noncalcareous components, and carbonate dissolution fueled by oxidation of organic matter.

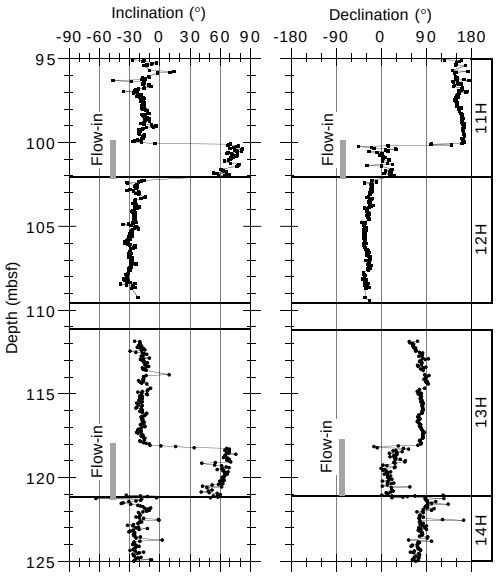

Figure 22. Example of remagnetization associated with sediment flow-in. Inclination of NRM and declination before correction of core orientation of Cores 175-1078D-11H through 14H.

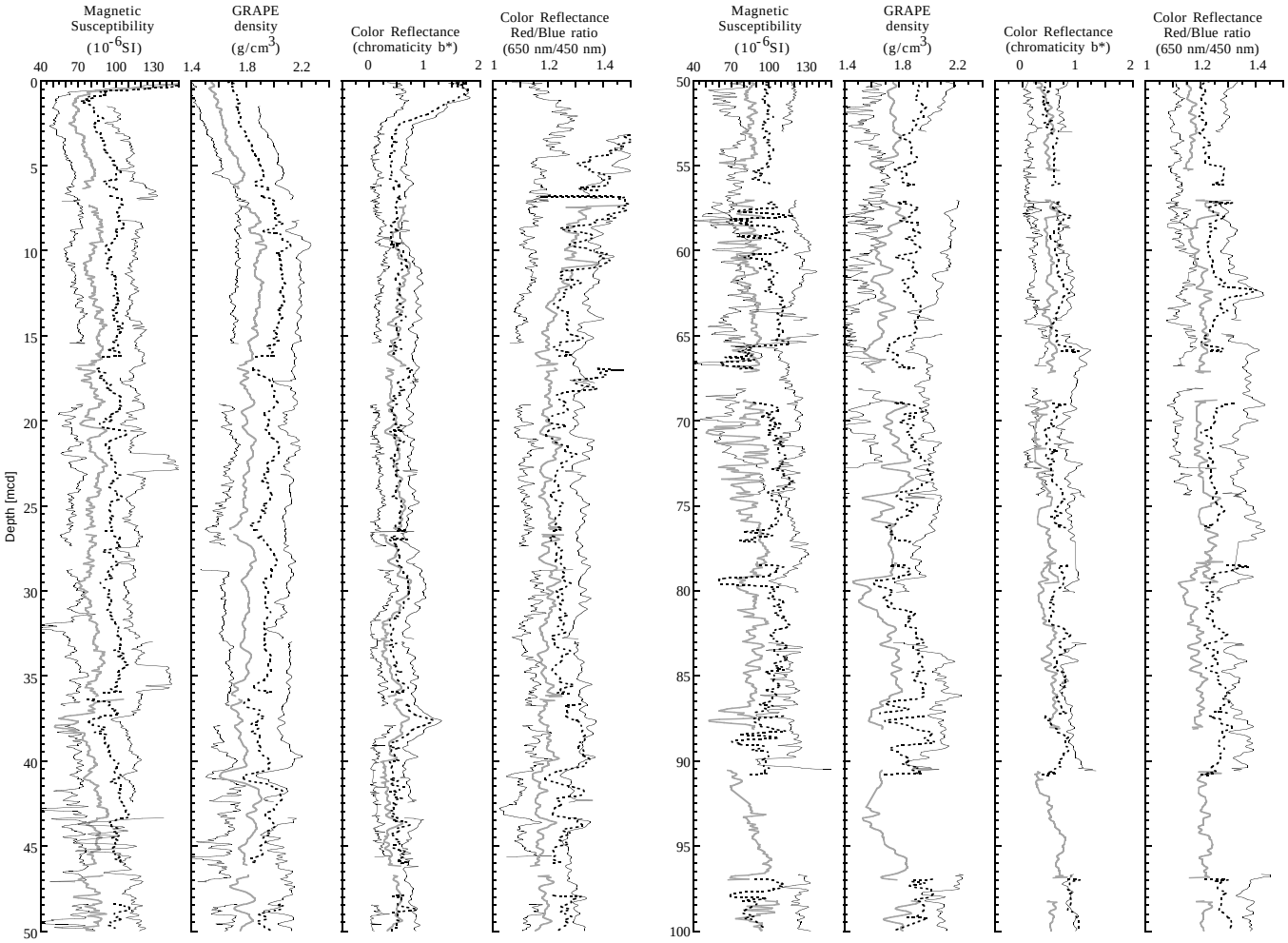

Figure 23. Composite section for Site 1078. Magnetic susceptibility, GRAPE density, and color reflectance (chromaticity b* and red/blue ratio [650 nm/450 nm]) data are plotted (left to right) for Holes 1078A (solid line), 1078B (gray line), 1078C (dashed line), and 1078D (solid black line). The down-hole logs are shown in meters composite depth (mcd). Offsets of integer multiples of 1.5 times the standard deviation of the Hole 1078A data have been applied to Holes 1078B, 1078C, and 1078D for clarity in viewing the composite section.

Table 7. Offsets applied to cores from Holes 1078A, 1078B, 1078C, and 1078D.

Core	Depth (mbsf)	Offset (m)	Composite depth (mcd)
175-1078A-			
1H	0.0	0.00	0.00
2H	7.5	–0.58	6.92
3H	17.0	1.96	18.96
4H	26.5	2.17	28.67
5H	36.0	1.84	37.84
6H	45.5	–0.65	44.85
7H	55.0	2.87	57.87
8H	64.5	2.62	67.12
9X	69.5	2.62	72.12
175-1078B-			
1H	0.0	0.00	0.00
2H	6.6	0.66	7.26
3H	16.1	0.73	16.83
4H	25.6	1.00	26.60
5H	35.1	1.20	36.30
6H	44.6	2.06	46.66
7H	54.1	1.16	55.26
8H	63.6	3.54	67.14
9H	73.1	4.67	77.77
10H	82.6	5.63	88.23
175-1078C-			
1H	0.0	0.00	0.00
2H	6.7	0.00	6.70
3H	16.2	0.63	16.83
4H	25.7	0.99	26.69
5H	35.2	1.08	36.28
6H	44.7	2.20	46.90
7H	54.2	1.35	55.55
8H	63.7	3.63	67.33
9H	73.2	4.79	77.99
10H	82.7	7.39	90.09
175-1078D-			
1H	0.0	–0.05	–0.05
2H	7.3	0.82	8.12
3H	16.8	0.63	17.43
4H	22.3	0.74	23.04
5H	31.8	1.10	32.90
6H	41.3	1.96	43.26
7H	50.8	–0.33	50.47
8H	60.3	4.19	64.49
9H	69.8	4.23	74.03
10H	79.3	0.39	79.69

Note: The offsets transform ODP standard depth values in meters below seafloor (mbsf) to meters composite depth (mcd).

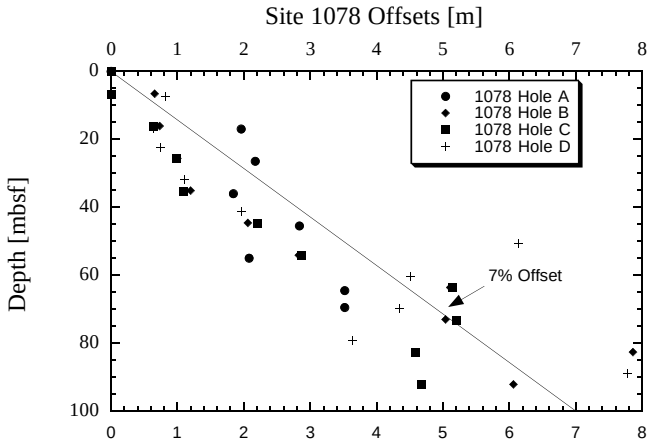

Figure 24. Core offsets applied to Site 1078 plotted against standard ODP meters below seafloor (mbsf). A linear 7% growth of meters composite depth (mcd) compared with mbsf is indicated by a line.

TOC determinations were done on a smaller number of Site 1078 sediment samples than carbonate determinations because of the generally uniform lithology. TOC values range from 1.06 to 5.35 wt% (Table 10) and average 2.53 wt%. The concentrations are nearly 10 times greater than the average of 0.3 wt% given by McIver (1975) based on DSDP Legs 1–33, a value that can be considered representative of typical deep-sea sediments. The high TOC concentrations at this site may be ascribed to a combination of a high supply of organic matter caused by elevated paleoproductivities and a high accumulation rate of sediments enhancing the preservation of organic matter.

Organic Matter Source Characterization

Organic C/N ratios were calculated for Site 1078 samples using TOC and total nitrogen concentrations to help identify the origin of their organic matter. Site 1078 C/N ratios vary from 9.3 to 15.7 (Table10). The C/N ratios average 12.1, a value that is intermediate between unaltered algal organic matter (5–8) and fresh land-plant material (25–35; e.g., Emerson and Hedges, 1988; Meyers, 1994). These organic carbon–rich sediments probably contain a mixture that is made up mostly of degraded algal material and partially of detrital continental organic matter. The C/N ratios that are higher than fresh algal organic matter reflect preferential loss of nitrogen-rich, proteinaceous matter and consequent elevation of C/N ratios during settling to the seafloor. This change in C/N ratios often occurs under areas of elevated algal productivity, such as the Angola margin (Meyers, 1997).

A Van Krevelen–type plot of hydrogen index (HI) and oxygen index (OI) values (Fig. 31) similarly indicates that the sediments contain type II (algal) organic matter that has been altered by microbial processing during early diagenesis. Well-preserved type II organic matter has high HI values (Peters, 1986), which can be lowered by microbial oxidation (Meyers, 1997). The low HI values of fresh type III organic matter, however, cannot become elevated by postdepositional alteration. Site 1078 sediments having higher Rock-Eval TOC values also have higher HI values (Fig. 32). This relationship confirms that the algal organic matter has been oxidized. Further evidence of substantial amounts of in situ organic matter degradation exists in the large increases in alkalinity and decreases in sulfate in the interstitial waters of Site 1078 sediments (see "Inorganic Geochemistry" section, this chapter).

Rock-Eval T_{max} values are low (Table 11), showing that organic matter is thermally immature with respect to petroleum generation (Peters, 1986). The low thermal maturity is consistent with the measured geothermal gradient of 45.7°C/km at this site (see "Physical Properties" section, this chapter).

Headspace Gases

Sediments from Site 1078 had high gas content. Gas pressures became great enough in sediments below Core 175-1078A-4H (36 mbsf) to require perforating the core liner to relieve the pressure and alleviate core expansion. Natural gas analyses determined that most of this gas was CO_2, and headspace concentrations of this gas continued to increase to the bottom of Hole 1078C (160 mbsf; Fig. 33). Hydrogen sulfide could be detected by nose, but not by hydrogen sulfide–sensing instruments having a sensitivity of ~1 ppm, in Cores 175-1078A-1H through 3H (1.5–26.5 mbsf).

Methane (C_1) first appears in headspace gas samples in Site 1078 sediments at 6 mbsf. Concentrations rapidly increase and become significant in sediments between 20 and 35 mbsf, below which they decrease (Fig. 34). As at Sites 1075, 1076, and 1077, high methane/ethane (C_1/C_2) ratios and the absence of major contributions of higher molecular weight hydrocarbon gases (Table 12) indicate that the gas is biogenic, as opposed to thermogenic, in origin. A biogenic origin of the methane is supported by the disappearance of interstitial sulfate at approximately the same sub-bottom depth where methane concentrations begin to rise (see "Inorganic Geochemistry" section, this chapter). As noted by Claypool and Kvenvolden (1983), the presence of interstitial sulfate inhibits methanogenesis in marine sediments.

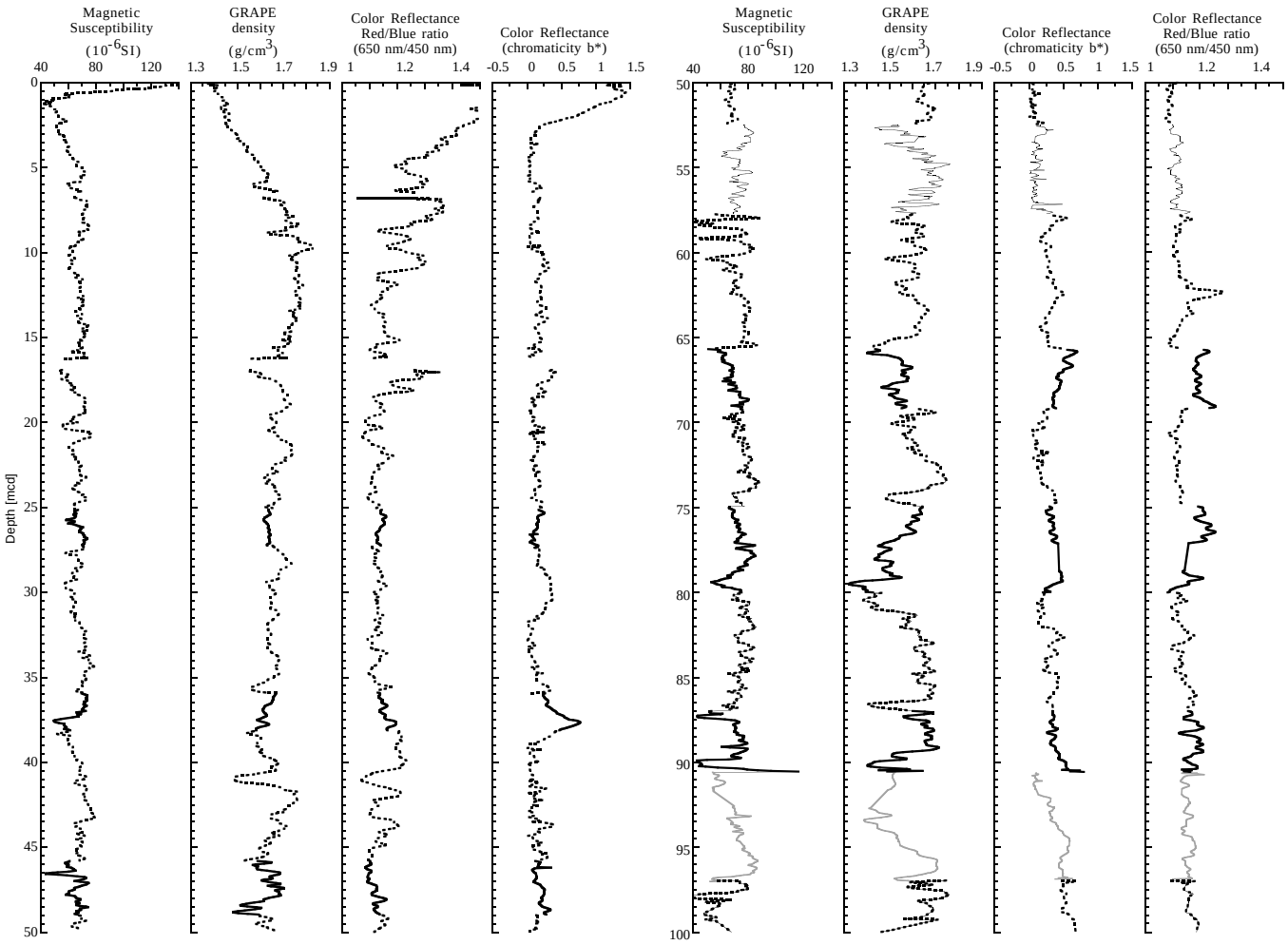

Figure 25. Spliced records for magnetic susceptibility, GRAPE density, and color reflectance (chromaticity b* and red/blue ratio [650 nm/450 nm]) are plotted in meters composite depth (mcd). Cores from four holes at Site 1078 have been used for the spliced record: thin solid line = Hole 1078A, gray line = Hole 1078B, dashed line = Hole 1078C, and thick solid line = Hole 1078D.

Table 8. List of splice tie points used to create the continuous "spliced" stratigraphic sequence for Site 1078.

Hole, core, section, interval (cm)	Depth (mbsf)	Composite depth (mcd)	Whether tied	Hole, core, section, interval (cm)	Depth (mbsf)	Composite depth (mcd)
1078C-1H-5, 44	6.44	6.44	Append	1078C-2H-1, 0	6.70	6.70
1078C-2H-7, 54	16.24	16.24	Append	1078C-3H-1, 0	16.20	16.83
1078C-3H-6, 80	24.50	25.13	Tie to	1078D-4H-2, 58.5	24.39	25.13
1078D-4H-3, 120	26.50	27.24	Tie to	1078C-4H-1, 52.5	26.25	27.24
1078C-4H-7, 24	34.94	35.93	Tie to	1078D-5H-3, 2.5	34.83	35.93
1078D-5H-4, 72	37.02	38.12	Tie to	1078C-5H-2, 44	37.04	38.12
1078C-5H-7, 60	44.70	45.78	Tie to	1078D-6H-2, 101	43.82	45.78
1078D-6H-4, 120	47.00	48.96	Tie to	1078C-6H-2, 56	46.76	48.96
1078C-6H-4, 104	50.24	52.44	Tie to	1078A-6H-4, 47	49.60	52.44
1078A-6H-7, 128	54.86	57.70	Tie to	1078C-7H-1, 58	54.84	57.70
1078C-7H-6, 108	62.78	65.64	Tie to	1078D-8H-1, 80	61.14	65.64
1078D-8H-3, 136	64.66	69.16	Tie to	1078C-8H-1, 32	64.02	69.16
1078C-8H-5, 8	69.78	74.92	Tie to	1078D-9H-1, 77	70.58	74.92
1078D-9H-4, 136	75.66	80.00	Tie to	1078C-9H-2, 9	74.80	80.00
1078C-9H-6, 104	81.74	86.94	Tie to	1078D-10H-4, 36	83.30	86.94
1078D-10H-6, 98	86.92	90.56	Append	1078B-10H-1, 0	82.60	90.46
1078B-10H-5, 64	89.14	97.00	Append	1078C-11H-1, 0	92.20	96.87
1078C-11H-7, 80	102.00	106.67				

Note: The tie points are listed in standard ODP meters below seafloor (mbsf) and meters composite depth (mcd).

Table 9. Interstitial water composition for Holes 1078A, 1078B, and 1078C.

Core, section, interval (cm)	Depth (mbsf)	pH	Alkalinity (mM)	Salinity	Cl^- (titr) (mM)	Cl^- (IC) (mM)	SO_4^{2-} (mM)	Na^+ (mM)	Mg^{2+} (mM)	Ca^{2+} (mM)	K^+ (mM)	H_4SiO_4 (µM)	NH_4^+ (µM)	PO_4^{3-} (µM)	Sr^{2+} (µM)
175-1078A-															
1H-1, 140-150	1.40	7.63	5.587	35.0	549	552	25.80	468.8	53.09	9.70	12.05	199	231	15	88
1H-4, 140-150	5.90	7.81	14.030	34.5	556	553	18.71	479.3	51.08	6.89	11.84	417	1050	52	77
2H-3, 140-150	11.90	7.90	37.983	34.0	563	556	1.52	484.6	50.22	3.81	11.28	467	2968	143	62
3H-3, 140-150	21.40	7.74	43.199	34.5	563	568	0.97	489.5	50.23	3.31	11.87	527	4848	64	67
4H-3, 140-150	30.90	7.72	47.988	35.0	562	560	0.00	496.4	46.96	3.64	12.37	555	6021	70	86
5H-3, 130-140	40.30	7.77	51.850	35.0	557	557	0.50	502.7	42.51	4.20	13.78	665	7827	70	101
6H-4, 135-145	50.50	7.73	63.261	35.5	551	556	0.00	503.0	44.83	3.73	14.37	577	10322	69	97
7H-3, 130-140	59.30	7.76	72.504	35.5	551	554	0.00	508.0	47.04	3.61	14.42	508	11588	93	89
8H-3, 140-150	68.10	7.10	74.152	36.0	551	547	1.21	511.6	46.25	4.25	15.22	488	12873	46	93
175-1078B-															
7H-4, 130-140	58.80	7.24	71.946	35.5	549	570	2.85	513.6	45.73	3.73	14.39	529	12482	86	91
8H-4, 130-140	68.90	7.52	72.319	36.0	547	562	0.00	503.3	46.49	4.21	14.48	484	12873	68	92
9H-3, 140-150	76.20	7.57	71.889	36.0	547	553	0.51	509.9	43.26	4.32	14.72	540	15796	67	97
10H-3, 130-140	86.90	7.65	61.280	36.0	546	548	0.00	504.4	39.88	3.55	15.87	417	15070	64	91
11H-3, 145-155	96.60	7.19	81.691	36.0	549	553	0.00	519.8	43.66	4.66	14.04	473	14604	73	99
14H-2, 145-155	124.00	7.39	59.983	36.0	546	549	0.00	510.5	34.62	2.18	21.68	287	15461	40	76
175-1078C-															
17X-3, 140-150	150.00	7.69	86.476	36.0	546	553	0.39	529.9	39.53	4.29	16.11	540	14437	44	121

Note: Cl^- (titr) = analyzed by titration and Cl^- (IC) = analyzed by ion chromatography.

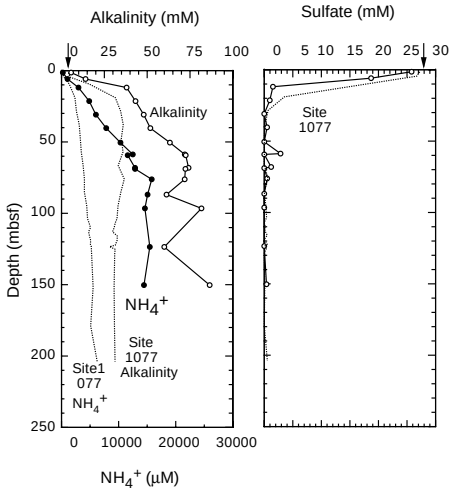

Figure 26. Downcore profiles of dissolved alkalinity (open circles) and ammonium (solid circles), and sulfate (right panel) at Site 1078. Arrows = mean ocean-bottom-water values taken from Millero and Sohn (1992). For comparison, profiles at Site 1077 (Congo Basin; dotted lines) are also shown.

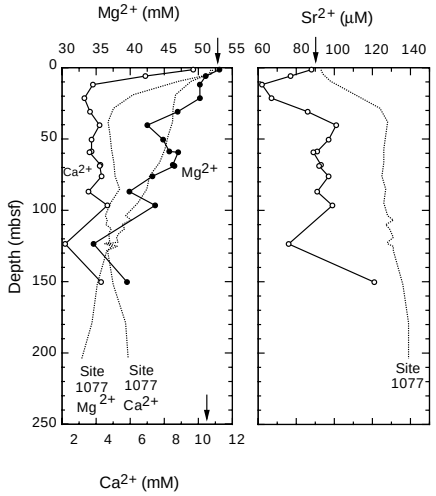

Figure 27. Downcore profiles of Ca^{2+} (open circles), Mg^{2+} (solid circles), and Sr^{2+} (right panel) at Site 1078. Arrows = mean ocean-bottom-water values taken from Millero and Sohn (1992). For comparison, profiles for Site 1077 (Congo Basin; dotted lines) are also shown.

PHYSICAL PROPERTIES

MST system measurements were made on whole-round sections of cores from each hole to determine GRAPE density, compressional (*P*-wave) ultrasonic velocity, magnetic susceptibility, and natural gamma radiation (see "Explanatory Notes" chapter, this volume). Some cores showed a high degree of disturbance at this site because of flow-in.

Index properties (gravimetric density) were measured on one or two samples (volume = ~10 cm^3) per working-half section on all cores from Hole 1078A using Method C (see "Explanatory Notes" chapter, this volume).

One or two ultrasonic compressional (*P*-wave) velocity and undrained vane-shear measurements per section were conducted close to the position of the discrete samples. For the discrete *P*-wave pulse-transmission experiments, the modified Hamilton Frame transducer system was used.

Multisensor Track

Sampling interval for GRAPE density (Fig. 35), ultrasonic compressional wave velocity (Fig. 36), and magnetic susceptibility (Fig. 37A) was 2 cm for the upper 50 mbsf and was changed to 4 cm below 50 mbsf. MST data are included on CD-ROM (back pocket, this volume). Natural gamma radiation measurements (NGR) were incorporated in the MST measurements, with a sampling period of 30 s at 32-cm resolution (Fig. 37B). Magnetic susceptibility and natural gamma radiation show some similarities (Fig. 37A and B, respectively), which may be attributed to higher proportions of clay including magnetic particles (see "Lithostratigraphy" section, this chapter). GRAPE density generally correlates well with the discrete wet bulk density data (Fig. 35).

Velocities

Discrete velocity measurements at Hole 1078A, determined with the Hamilton Frame, show velocities between 1460 and 1655 m/s

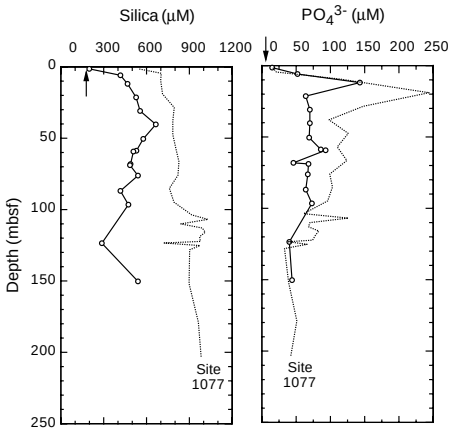

Figure 28. Downcore profiles of dissolved silica and phosphate at Site 1078 (open circles). Arrows = mean ocean-bottom-water values taken from Millero and Sohn (1992). For comparison, profiles for Site 1077 (Congo Basin; dotted lines) are also shown.

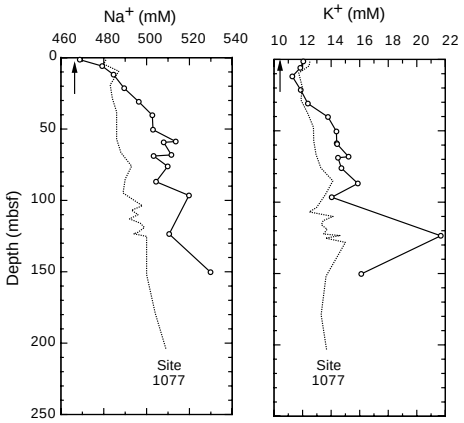

Figure 29. Downcore profiles of dissolved Na^+ and K^+ at Site 1078. Arrows = mean ocean-bottom-water values taken from Millero and Sohn (1992). For comparison, profiles for Site 1077 (Congo Basin; dotted lines) are also shown.

(Fig. 36). The velocity profile is similar to discrete density measurements (see below), which display higher values of silty clays (see "Lithostratigraphy" section, this chapter). The ultrasonic signals were completely attenuated below 26 mbsf, although down to this depth, signals could be recorded with high signal/noise ratio. Discrete velocity values match well with the MST compressional velocities in the upper 7 mbsf and then diverge toward higher values (Fig. 36).

Index Properties

Results of discrete measurements of wet bulk density, porosity, and moisture content for Hole 1078A are presented in Figures 38A, 38B, and 38C, respectively (also see Table 13 on CD-ROM, back pocket, this volume). The density values vary between 1380 and 1750 kg/m^3. Porosities decrease from 76% in the top section to <60% deeper in the hole. Between 0 and 25 mbsf, discrete density values are lower than those for the GRAPE measurements. Both data sets match very well between 25 and 40 mbsf; however, below 40 mbsf, discrete wet bulk density values are generally higher than GRAPE values. Both profiles are very similar in shape, revealing good coherence between the two types of measurements. Note the good correlation between the density and velocity profiles at this site.

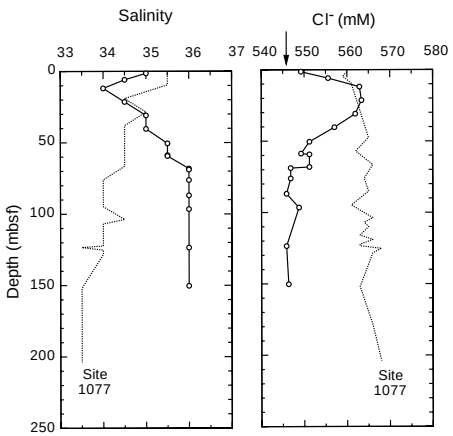

Figure 30. Downcore profiles of salinity and dissolved Cl^- at Site 1078 (solid line with open circles). Arrow = mean ocean-bottom-water value taken from Millero and Sohn (1992). For comparison, profiles for Site 1077 (Congo Basin; dotted lines) are also shown.

Thermal Conductivity and Geothermal Gradient

The thermal conductivity profile at Hole 1078A was measured at a resolution of one every second core section (see "Explanatory Notes" chapter, this volume). The values show little variation between 0 and 40 mbsf and show a decrease below that depth associated with a higher scatter (Fig. 37C).

At Site 1078, the Adara tool was deployed to measure formation temperature. A preliminary analysis provided three data points, which were used to estimate a geothermal gradient of 46°C/km, but further analyses will be required to confirm this result.

Vane Shear Strength

An undrained vane-shear measurement was usually performed in the bottom part of each core section. The profile shows a gradual increase of shear strength down to 42 mbsf (Fig. 37D). Below 42 mbsf, values show higher scatter significantly, which may be dependent on the position relative to the top or base of the cores where degassing and voids are most pronounced and low vane-shear values are expected (core breaks are indicated in Fig. 37D for comparison). Maximum values may represent less disturbed sections; their increase indicates compaction with depth. The shear-strength profile reveals an overall match with the wet bulk density profile.

REFERENCES

Baumgartner, T.R., and van Andel, T.H., 1971. Diapirs of the continental margin of Angola, Africa. *Geol. Soc. Am. Bull.*, 82:793–802.

Berger, W.H., and Wefer, G., 1991. Productivity of the glacial ocean: discussion of the iron hypothesis. *Limnol. Oceanogr.*, 36:1899–1918.

Berggren, W.A., Kent, D.V., Swisher, C.C., III, and Aubry, M.-P., 1995. A revised Cenozoic geochronology and chronostratigraphy. *In* Berggren, W.A., Kent, D.V., Aubry, M.-P., and Hardenbol, J. (Eds.), *Geochronology, Time Scales and Global Stratigraphic Correlation.* Spec. Publ.—Soc. Econ. Paleontol. Mineral. (Soc. Sediment. Geol.), 54:129–212.

Bleil, U., and Shipboard Scientific Party, 1995. Report and preliminary results of SONNE cruise SO 86. *Ber. Fachber. Geowiss.*, Univ. Bremen, 51.

Bolli, H.M., Ryan, W.B.F., et al., 1978. *Init. Repts. DSDP,* 40: Washington (U.S. Govt. Printing Office).

Boltovskoy, E., 1972. Nota sobre los valores mínimos de oxigenación que pueden soportar los foraminíferos bentónicos. *Bol. Soc. Biol. Concepcion*, 45:135–143.

Brice, S.E., Cochran, M.D., Pardo, G., and Edwards, A.D., 1982. Tectonics and sedimentation of the South Atlantic Rift Sequence: Cabinda, Angola.

Table 10. Percentages of inorganic and total carbon, total nitrogen, and total sulfur in sediment samples from Holes 1078A, 1078B, and 1078C.

Core, section, interval (cm)	Depth (mbsf)	IC (wt%)	$CaCO_3$ (wt%)	TC (wt%)	TOC (wt%)	TN (wt%)	TS (wt%)	C/N (atomic)
175-1078A-								
1H-1, 46-47	0.46	2.02	16.84	6.08	4.05	0.42	0.52	11.4
1H-3, 46-47	3.46	2.08	17.34	4.23	2.14	0.22	0.86	11.4
1H-5, 46-47	6.46	1.74	14.47	3.61	1.87	0.19	0.62	11.5
2H-1, 46-47	7.96	3.05	25.39	4.11	1.06	0.13	0.67	9.3
2H-3, 46-47	10.96	2.13	17.75	4.42	2.29	0.21	0.93	12.6
2H-5, 46-47	13.96	2.07	17.26					
3H-1, 46-47	17.46	1.95	16.23					
3H-3, 46-47	20.46	2.04	17.03	4.55	2.51	0.23	1.28	12.7
3H-5, 46-47	23.46	1.69	14.07					
4H-1, 46-47	26.96	2.50	20.86					
4H-3, 46-47	29.96	1.76	14.67	4.72	2.95	0.26	1.54	13.1
4H-5, 46-47	32.96	2.22	18.49					
5H-1, 46-47	36.46	2.13	17.77					
5H-2, 30-31	37.83	2.43	20.20	4.39	1.96	0.22	1.53	10.2
5H-3, 46-47	39.49	1.69	14.04					
5H-5, 48-49	42.41	2.05	17.10	4.24	2.18	0.20	1.37	12.9
6H-2, 46-47	46.57	1.77	14.78					
6H-4, 46-47	49.58	1.55	12.87	4.44	2.89	0.25	1.43	13.5
6H-6, 46-47	52.54	2.01	16.76					
7H-1, 46-47	55.46	2.01	16.70					
7H-3, 46-47	58.48	2.04	17.02	5.53	3.48	0.30	1.31	13.7
7H-5, 46-47	61.38	1.73	14.38					
8H-1, 46-47	64.96	2.23	18.57					
8H-3, 46-47	67.20	2.11	17.61	4.79	2.68	0.26	1.58	12.0
8H-5, 46-47	69.16	2.01	16.71					
175-1078B-								
8H-1, 46-47	64.06	1.92	16.01					
8H-3, 46-47	66.55	1.94	16.16	4.17	2.23	0.21	1.41	12.3
8H-5, 46-47	69.45	2.11	17.60	4.32	2.20	0.20	1.27	13.2
9H-3, 46-47	75.24	0.15	1.28	5.50	5.35	0.43	1.67	14.5
9H-5, 46-47	78.24	0.38	3.15	4.94	4.56	0.38	1.74	14.2
10H-1, 46-47	83.06	1.80	14.96	3.43	1.63	0.16	0.93	11.9
10H-3, 46-47	86.06	1.95	16.22	3.40	1.45	0.17	0.97	10.0
10H-5, 46-47	88.96	2.11	17.60					
11H-1, 46-47	92.56	2.14	17.82					
11H-3, 46-47	95.56	1.82	15.15	4.15	2.33	0.23	0.93	12.0
11H-5, 46-47	98.61	2.46	20.48					
12H-1, 46-47	102.06	0.40	3.35	4.81	4.41	0.37	1.49	14.0
12H-3, 46-47	105.06	1.81	15.09					
12H-6, 46-47	108.09	1.19	9.89	2.30	1.11	0.13	0.86	10.2
13H-1, 46-47	111.56	1.90	15.83					
13H-3, 37-38	113.84	1.51	12.54					
13H-5, 46-47	115.75	1.66	13.85	3.98	2.32	0.23	1.09	11.6
14H-1, 46-47	121.06	1.41	11.73					
14H-3, 46-47	124.06	2.25	18.73					
14H-5, 46-47	127.11	1.66	13.85	3.55	1.89	0.21	1.47	10.5
175-1078C-								
15X-1, 46-47	129.26	1.50	12.53	3.39	1.88	0.19	1.06	11.5
15X-3, 46-47	132.26	0.71	5.95	4.02	3.31	0.28	1.62	13.8
16X-1, 46-47	136.66	1.89	15.77					
17X-1, 46-47	146.36	1.32	10.98	4.23	2.91	0.22	1.18	15.7
17X-3, 46-47	149.36	1.72	14.31	3.68	1.97	0.23	1.33	10.0
17X-5, 46-47	152.36	1.20	9.96	3.68	2.49	0.24	1.42	12.3
18X-1, 46-47	155.96	0.98	8.16					
18X-3, 46-47	158.96	1.02	8.49	2.95	1.93	0.19	1.26	11.9
18X-4, 46-47	160.46	0.89	7.41	2.69	1.80	0.20	1.06	10.6

Notes: IC = inorganic carbon; $CaCO_3$ = calcium carbonate; TC = total carbon; TOC = total organic carbon; TN = total nitrogen; TS = total sulfur; and C/N = carbon/nitrogen ratio; Blanks = no data available. TOC concentrations are calculated from the difference between IC and TC concentrations. C/N ratios are calculated from TOC and TN concentrations and are given as atom/atom ratios.

In Watkins, J.S., and Drake, C.L. (Eds.), *Studies in Continental Margin Geology.* AAPG Mem., 34:5–18.

Claypool, G.E., and Kvenvolden, K.A., 1983. Methane and other hydrocarbon gases in marine sediment. *Annu. Rev. Earth Planet. Sci.*, 11:299–327.

Emerson, S., and Hedges, J.I., 1988. Processes controlling the organic carbon content of open ocean sediments. *Paleoceanography*, 3:621–634.

Emery, K.O., and Uchupi, E., 1984. *The Geology of the Atlantic Ocean:* New York (Springer-Verlag).

Emery, K.O., Uchupi, E., Phillips, J., Bowin, C., and Mascle, J., 1975. Continental margin off Western Africa: Angola to Sierra Leone. *AAPG Bull.*, 59:2209–2265.

Hentschel, E., 1933. Allgemeine Biologie des südatlantischen Ozeans. *Wiss. Erg. Dt. Atl. METEOR Exped.*, 11:1–168.

Jansen, J.H.F., Ufkes, E., and Schneider, R.R., 1996. Late Quaternary movements of the Angola-Benguela-Front, SE Atlantic, and implications for advection in the equatorial ocean. *In* Wefer, G., Berger, W.H., Siedler, G., and Webb, D. (Eds.), *The South Atlantic: Present and Past Circulation:* Berlin (Springer-Verlag), 553–575.

Jansen, J.H.F., and Van Iperen, J.M., 1991. A 220,000-year climatic record for the east equatorial Atlantic Ocean and equatorial Africa: evidence from diatoms and opal phytoliths in the Zaire (Congo) deep-sea fan. *Paleoceanography*, 6:573–591.

Leyden, R., Bryan, G., and Ewing, M., 1972. Geophysical reconaissance on African Shelf: 2. Margin sediments from Gulf of Guinea to Walvis Ridge. *AAPG Bull.*, 56:682–693.

Martini, E., 1971. Standard Tertiary and Quaternary calcareous nannoplankton zonation. *In* Farinacci, A. (Ed.), *Proc. 2nd Int. Conf. Planktonic Microfossils Roma:* Rome (Ed. Tecnosci.), 2:739–785.

McIver, R.D., 1975. Hydrocarbon occurrences from JOIDES Deep Sea Drilling Project. *Proc. Ninth Petrol. Congr.*, 269–280.

Meyers, P.A., 1994. Preservation of elemental and isotopic source identification of sedimentary organic matter. *Chem. Geol.*, 144:289–302.

————, 1997. Organic geochemical proxies of paleoceanographic, paleolimnologic, and paleoclimatic processes. *Org. Geochem.*, 27:213–250.

Millero, F.J., and Sohn, M.L., 1992. *Chemical Oceanography:* Boca Raton (CRC Press).

Okada, H., and Bukry, D., 1980. Supplementary modification and introduction of code numbers to the low-latitude coccolith biostratigraphic zonation (Bukry, 1973; 1975). *Mar. Micropaleontol.*, 5:321–325.

Peters, K.E., 1986. Guidelines for evaluating petroleum source rock using programmed pyrolysis. *AAPG Bull.*, 70:318–329.
Phleger, F., and Soutar, A., 1973. Production of benthic foraminifera in three east Pacific oxygen minima. *Micropaleontology,* 19:110–115.
Roberts, A.P., Stoner, J.S., and Richter, C., 1996. Coring induced magnetic overprints and limitations of the long-core paleomagnetic measurements technique: some observations from Leg 160, eastern Mediterranean Sea. *In* Emeis, K.-C., Robertson, A.H.F., Richter, C., et al., *Proc. ODP, Init. Repts.*, 160: College Station, TX (Ocean Drilling Program), 497–505.
Schneider, R.R., Price, B., Müller, P.J., Kroon, D., and Alexander, I., 1997. Monsoon related variations in Zaire (Congo) sediment load and influence of fluvial silicate supply on marine productivity in the east equatorial Atlantic during the last 200,000 years. *Paleoceanography,* 12:463–481.
Sellier de Civrieux, J.M., and Bonilla, J., 1971. La influencia de los parámetros físico-químicos del fondo en las facies de foraminíferos bentónicos. *Univ Oriente, Inst. Oceanogr. Bol.,* 9:15–34.
Shannon, L.V., and Pillar, S.C., 1986. The Benguela Ecosystem, III, Plankton. *Oceanogr. Mar. Biol.,* 24:65–170.
Smith, P.B., 1963. Quantitative and qualitative analysis of the family Bolivinidae. *Geol. Surv. Prof. Pap. U.S.,* 429A:A1–A39.
————, 1964. Ecology of benthonic species. *Geol. Surv. Prof. Pap. U.S.*, 429–B.
Van Bennekom, A.J., and Berger, G.W., 1984. Hydrography and silica budget of the Angola Basin. *Neth. J. Sea Res.*, 17:149–200.
van der Gaast, S.J., and Jansen, J.H.F., 1984. Mineralogy, opal, and manganese of Middle and Late Quaternary sediments of the Zaire (Congo) deep-sea fan: origin and climatic variation. *Neth. J. Sea Res.*, 17:313–341.
Weaver, P.P.E., 1993. High resolution stratigraphy of marine Quaternary sequences. *In* Hailwood, E.A., and Kidd, R.B. (Eds.), *High Resolution Stratigraphy.* Geol. Soc. Spec. Publ. London, 70:137–153.
Wefer, G., and Shipboard Scientific Party, 1988. Bericht über die METEOR-Fahrt M6/6, Libreville - Las Palmas, 18.2–23.3. 1988. *Ber. Fachbereich Geowiss. Univ. Bremen, Germany,* 3.

Ms 175IR-106

NOTE: Core-description forms ("barrel sheets") and core photographs can be found in Section 4, beginning on page 581. Forms containing smear-slide data can be found on CD-ROM. See Table of Contents for materials contained on CD-ROM.

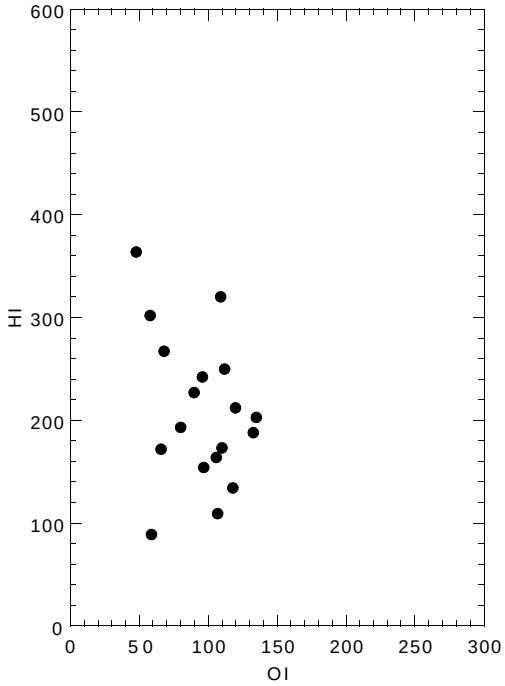

Figure 31. Rock-Eval Van Krevelen–type diagram of sediments from Holes 1078A, 1078B, and 1078C. Organic matter appears to be predominantly type II algal material that has been variably oxidized. HI = milligrams of hydrocarbons per gram of organic carbon; OI = milligrams of CO_2 per gram of organic carbon.

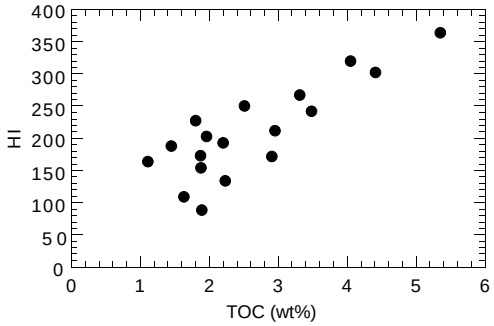

Figure 32. Comparison of Rock-Eval hydrogen index (HI) values and TOC concentrations of sediments from Holes 1078A, 1078B, and 1078C. The correspondence between increases in both parameters indicates that preservation of marine organic matter is important in enhancing the organic carbon richness of sediments on the Angola margin.

Table 11. Results of Rock-Eval pyrolysis analyses of sediments from Holes 1078A, 1078B, and 1078C.

Core, section, interval (cm)	Depth (mbsf)	TOC (wt%)	S_1	S_2	S_3	T_{max} (°C)	HI	OI
175-1078A-								
1H-1, 46-47	0.46	4.05	2.22	12.97	4.43	414	320	109
1H-5, 46-47	6.46	1.87	0.43	3.25	2.07	417	173	110
3H-3, 46-47	20.46	2.51	0.61	6.30	2.83	420	250	112
4H-3, 46-47	29.96	2.95	0.76	6.27	3.54	414	212	120
5H-2, 30-31	37.83	1.96	0.4	3.99	2.66	420	203	135
7H-3, 46-47	58.48	3.48	0.78	8.45	3.36	419	242	96
175-1078B-								
8H-3, 46-47	66.55	2.23	0.31	2.99	2.65	423	134	118
8H-5, 46-47	69.45	2.20	0.53	4.26	1.76	414	193	80
9H-3, 46-47	75.24	5.35	1.60	19.52	2.60	415	364	48
10H-1, 46-47	83.06	1.63	0.22	1.78	1.76	419	109	107
10H-3, 46-47	86.06	1.45	0.29	2.74	1.93	422	188	133
12H-1, 46-47	102.06	4.41	0.91	13.34	2.60	423	302	58
12H-6, 46-47	108.09	1.11	0.23	1.83	1.18	414	164	106
14H-5, 46-47	127.11	1.89	0.17	1.69	1.13	423	89	59
175-1078C-								
15X-1, 46-47	129.26	1.88	0.31	2.90	1.83	421	154	97
15X-3, 46-47	132.26	3.31	1.25	8.84	2.26	406	267	68
17X-1, 46-47	146.36	2.91	0.36	5.03	1.94	426	172	66
18X-4, 46-47	160.46	1.80	0.40	4.10	1.62	422	227	90

Notes: TOC = total organic carbon; HI = hydrogen index; and OI = oxygen index. Units of the various Rock-Eval parameters are given in the "Organic Geochemistry" section of the "Explanatory Notes" chapter (this volume).

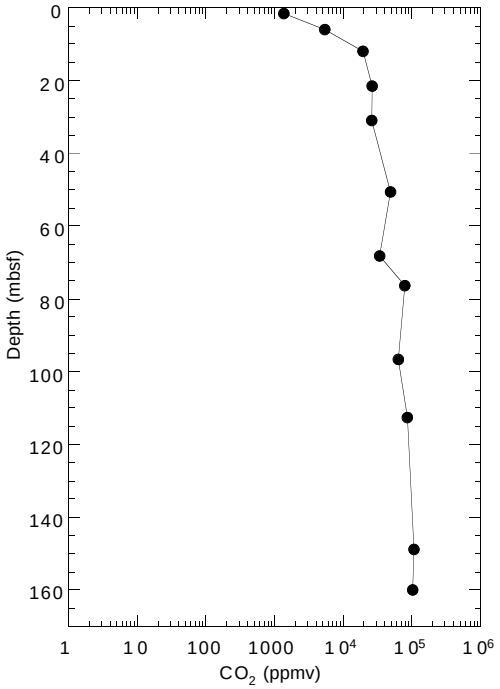

Figure 33. Headspace CO_2 concentrations in sediments from Holes 1078A, 1078B, and 1078C.

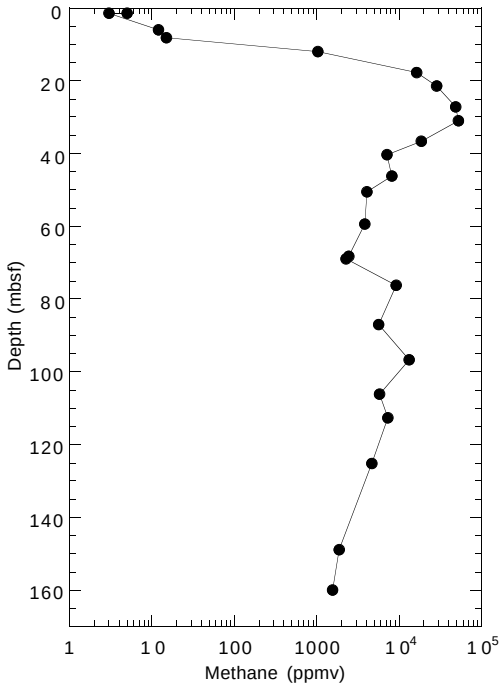

Figure 34. Headspace methane concentrations in sediments from Holes 1078A, 1078B, and 1078C.

Table 12. Results of headspace gas analyses of sediments from Holes 1078A, 1078B, and 1078C.

Core, section, interval (cm)	Depth (mbsf)	C_1 (ppmv)	CO_2 (ppmv)	C_2= (ppmv)	C_2 (ppmv)	C_3 (ppmv)	C_1/C_2
175-1078A-							
1H-2, 0-5	1.50	3	1,356				
1H-5, 0-5	6.00	12	5,365		0.1		120
2H-4, 0-5	12.00	1,029	19,258		0.4		2,573
3H-4, 0-5	21.50	28,466	26,433		1.3	0	21,897
4H-4, 0-5	31.00	53,024	25,891	0.2	3.0	1	17,675
5H-4, 0-5	40.43	7,128			1.0	0	7,128
6H-5, 0-5	50.57	4,109	48,670		0.7	1	5,870
7H-4, 0-5	59.42	3,825		0.1	0.9	1	4,250
8H-4, 0-5	68.24	2,448	33,684		0.4	0	6,120
175-1078B-							
8H-5, 0-5	68.99	2,280			0.5	0	4,560
9H-4, 0-5	76.28	9,225	78,421		2.4	0	3,844
10H-4, 0-5	87.00	5,724		0.2	1.0	1	5,724
11H-4, 0-5	96.65	13,220	63,710	0.3	2.9	1	4,559
12H-4, 0-5	106.10	5,836			1.0	0	5,836
13H-2, 0-5	112.60	7,367	85,846	0.1	2.9	1	2,540
14H-4, 0-5	125.15	4,692		0.1	1.5	0	3,128
175-1078C-							
1H-2, 0-5	1.50	5					
2H-2, 0-5	8.20	15					
3H-2, 0-5	17.70	16,301			0.9		18,112
4H-2, 0-5	27.20	48,766		0.2	3.0	1	16,255
5H-2, 0-5	36.60	18,749		0.2	2.3	2	8,152
6H-2, 0-5	46.20	8,243			1.6	1	5,152
17X-3, 0-5	148.90	1,883	107,628	0.4	3.3	2	571
18X-4, 0-5	160.00	1,557	102,936	0.2	3.4	1	458

Notes: C_1 = methane; CO_2 = carbon dioxide; C_2= = ethene; C_2 = ethane; C_3 = propane. Dominance of C_1 over C_2 indicates that the gases originate from in situ microbial degradation of organic matter.

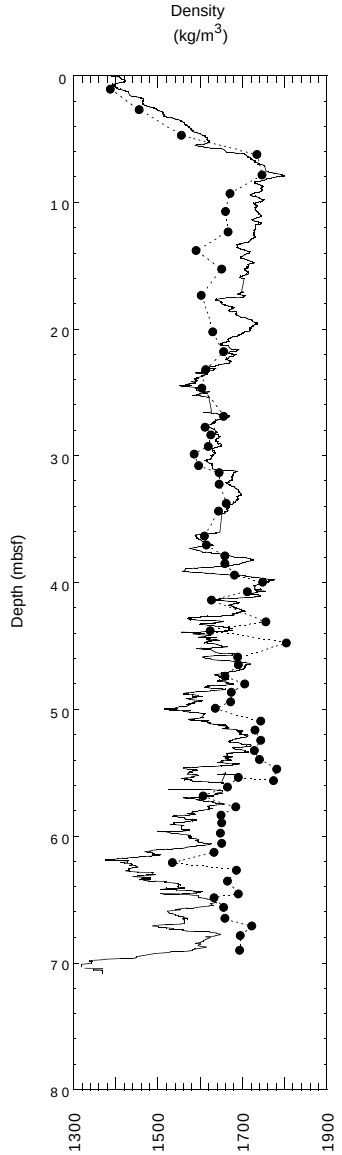

Figure 35. Discrete wet bulk density values (solid circles) compared with the GRAPE density profile (solid line) for Hole 1078A.

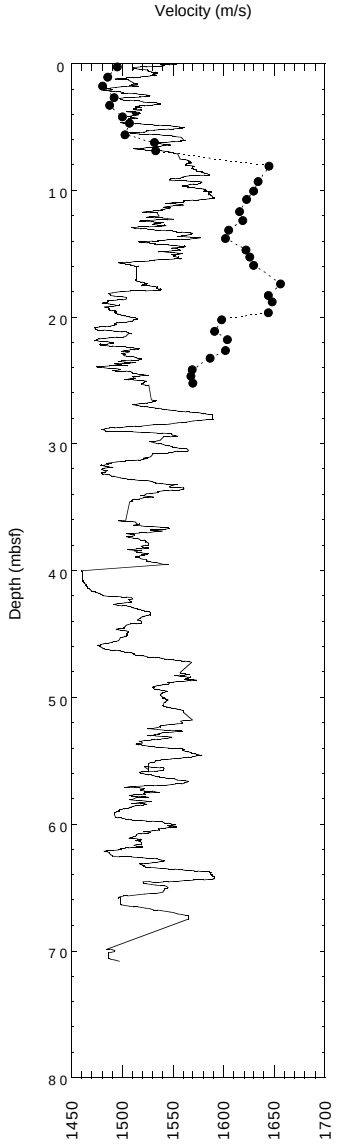

Figure 36. Discrete (solid circles) and MST (solid line) velocity measurements for Hole 1078A.

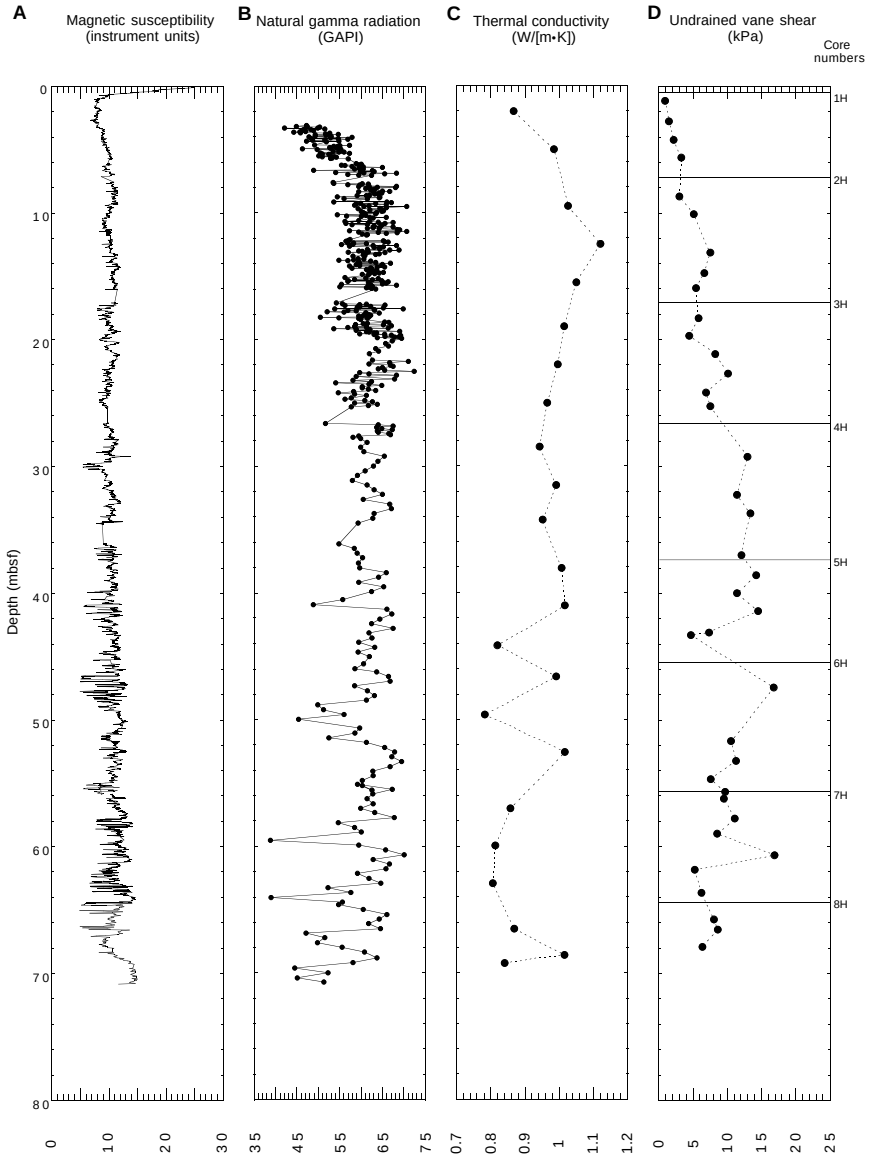

Figure 37. Plots of (**A**) magnetic susceptibility and (**B**) natural gamma radiation from MST measurements compared with discrete values of (**C**) thermal conductivity and (**D**) undrained vane-shear strength for Hole 1078A.

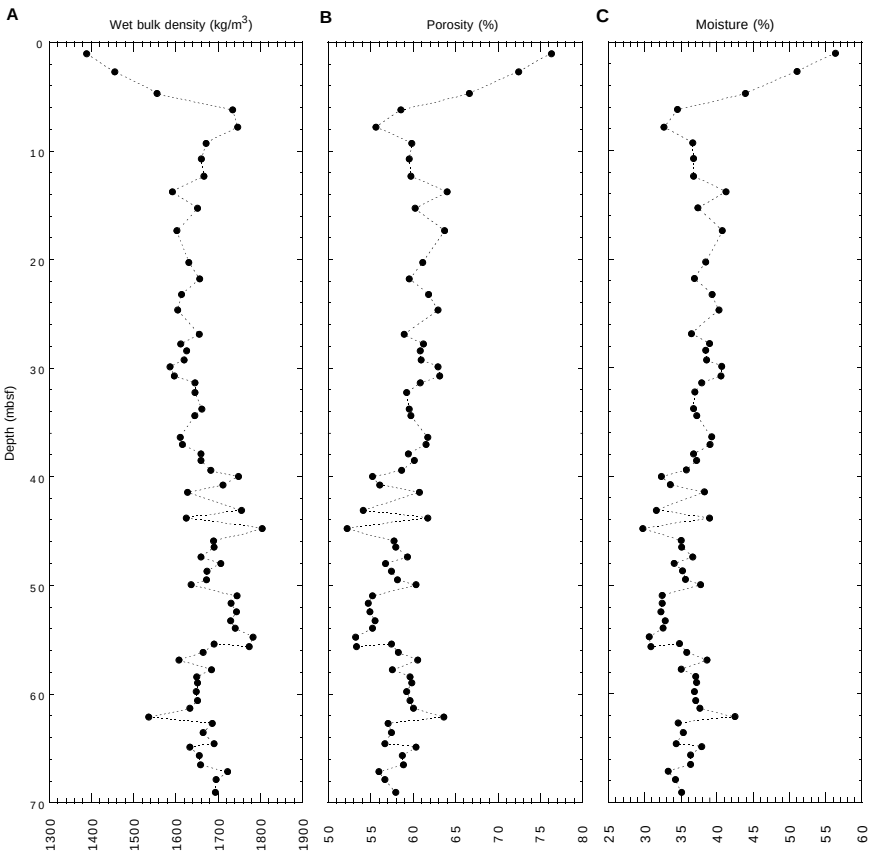

Figure 38. Plots of (**A**) wet bulk density, (**B**) porosity, and (**C**) moisture content derived from index properties measurements for Hole 1078A.